Garnet and zircon geochronology of the Paleoproterozoic Kuru-Vaara eclogites, northern Belomorian Province, Fennoscandian Shield

Aleksey E. Melnik[a,b,*], Sergey G. Skublov[b,c], Daniela Rubatto[d,e], Dirk Müller[f], Xian-Hua Li[a], Qiu-Li Li[a], Aleksey V. Berezin[b,g], Daniel Herwartz[h], Maria M. Machevariani[c]

[a] *State Key Laboratory of Lithospheric Evolution, Institute of Geology and Geophysics, Chinese Academy of Sciences, Beitucheng West Road 19, Beijing 100029, China*

[b] *Institute of Precambrian Geology and Geochronology, Russian Academy of Sciences, nab. Makarova 2, St. Petersburg 199034, Russia*

[c] *Saint-Petersburg Mining University, 21-ya Liniya 2, St. Petersburg 199106, Russia*

[d] *Institute of Geological Sciences, University of Bern, Baltzerstrasse 1+3, 3012 Bern, Switzerland*

[e] *Institute of Earth Sciences, University of Lausanne, Géopolis, Quartier Mouline, 1015 Lausanne, Switzerland*

[f] *Department of Earth and Environmental Sciences, Ludwig-Maximilians-Universität München, Theresienstr. 41, Munich 80333, Germany*

[g] *Saint-Petersburg State University, nab. Universitetskaya 7-9, St. Petersburg 199034, Russia*

[h] *Institut für Geologie und Mineralogie, Universität Köln, Zülpicherstr. 49b, Köln D-50674, Germany*

* Corresponding author: Aleksey E. Melnik, e-mail: aleksei@mail.iggcas.ac.cn

State Key Laboratory of Lithospheric Evolution, Institute of Geology and Geophysics, Chinese Academy of Sciences, Beitucheng West Road 19, Beijing 100029, China

Abstract

The Belomorian Province of the Fennoscandian Shield exposes numerous Precambrian eclogites, which makes it significant for the study of early tectonic processes. The age of these eclogites has been discussed for more than 15 years and regarded as either Archean or Paleoproterozoic. In the Kuru-Vaara quarry within the northern Belomorian Province, the eclogitic assemblage is preserved in concordant mafic boudins in felsic gneisses and a partially eclogitized gabbro-norite dike cutting discordantly through the gneiss fabric. Both eclogite types preserve zircon cores with a magmatic geochemical signature that yield protolith ages of ca. 2.88 Ga for a mafic boudin and ca. 2.44 Ga for the eclogitized gabbro-norite. Ca. 1.9 Ga zircon rims and grains from the eclogites show low Th/U ratio and HREE depletion, reflecting the growth of metamorphic zircon in equilibrium with garnet. In the eclogite boudin, the Archean zircon cores yield $\delta^{18}O$ = 5.1-5.9‰ typical of mantle melts; the oxygen isotope composition of garnet ($\delta^{18}O$ = 4.0-5.0‰) is in equilibrium with that of the 1.9 Ga zircon ($\delta^{18}O$ = 4.5-5.4‰). Garnet Lu-Hf geochronology coupled with U-Pb zircon geochronology constrains prograde metamorphism for the Kuru-Vaara eclogites at 1.92-1.89 Ga. Mineral inclusions of garnet, zoisite, plagioclase, kyanite, amphibole, quartz, and low-Na clinopyroxene in ca. 1.9 Ga zircon from the eclogite boudin imply epidote-amphibolite/amphibolite facies conditions for the prograde metamorphism. All data point to a Paleoproterozoic age of the eclogite facies metamorphism.

Keywords. Kuru-Vaara; ancient eclogites; zircon dating; garnet dating; oxygen isotopes; eclogitized gabbro-norite

1. Introduction

It is still debated how plate tectonics has operated in early Earth's history and when subduction-collision processes have begun (e.g., Brown, 2006, 2008, 2009; Condie and Kröner, 2008;

Sizova et al., 2010; van Hunen and Moyen, 2012). Subduction tectonics in the Archean has been proposed by some studies on the basis of geochemical and geological evidence (e.g., Abbott et al., 1994; Brown, 2006; Condie and Kröner, 2008). Formed in subduction-collision zones, crustal eclogites occur in orogenic belts and represent a reliable proxy for plate tectonics (e.g., Brown, 2014). Therefore, the oldest eclogites are pivotal for setting constraints on the starting time of subduction processes similar to those that operate on modern Earth. The earliest crustal eclogites are Paleoproterozoic and they occur in a limited number of orogenic belts: the Eburnian-Transamazonian orogen (ca. 2.09 Ga, Loose and Schenk, 2018); the Kasai Block of the Congo Craton (ca. 2.09 Ga, François et al., 2018); the Usagaran belt (ca. 2.00 Ga, Collins et al., 2004; Möller et al., 1995); the Ubendian belt (ca. 1.89-1.87 Ga, Boniface et al., 2012); the Snowbird tectonic zone (ca. 1.90 Ga, Baldwin et al., 2004); the Trans-Hudson orogen (ca. 1.83 Ga, Weller and St-Onge, 2017); the Nagssugtoqidian Orogen, South-East Greenland (ca. 1.89-1.88 Ga, Müller et al., 2018).

Early Precambrian eclogites are also widespread within the Belomorian Province of the Fennoscandian Shield. These rocks have caught much attention since Archean zircon ages of 2.87-2.72 Ga were interpreted as dating high pressure metamorphism of the Salma and Gridino eclogites (Mints et al., 2010; Volodichev et al., 2004). Subsequently, based on zircon U-Pb geochronology and garnet Sm-Nd and Lu-Hf geochronology, the Belomorian Province eclogites were identified as Paleoproterozoic with an age of ca. 1.9 Ga (e.g., Berezin et al., 2012; Herwartz et al., 2012; Imayama et al., 2017; Li et al., 2017a; Liu et al., 2017; Mel'nik et al., 2013; Skublov et al., 2010, 2011a, 2011b; Yu et al., 2017, 2019a). However, the age of eclogite facies metamorphism in the Belomorian Province is still regarded as Archean in some recent studies (Dokukina and Mints, 2019; Mints and Dokukina, 2020).

This contribution focuses on eclogites from the Kuru-Vaara quarry of the Salma area which age is equally disputed. Based on geological observations and zircon U-Pb dating, an unspecified Neoarchean age was inferred for Kuru-Vaara eclogites (Balagansky et al., 2015; Shchipansky et al.,

2012a, 2012b). These studies considered the cross-cutting relationship between an early Paleoproterozoic dike of gabbro-norite and the eclogite bearing mélange as an evidence for Archean eclogite metamorphism since an eclogite assemblage has not been identified in the dike. An age of ca. 1.9 Ga was suggested to peak eclogite facies metamorphism (Herwartz et al., 2012; Mel'nik et al., 2013; Skublov et al., 2010, 2011b) or prograde eclogite facies stage (Liu et al., 2017) based on Sm-Nd and Lu-Hf dating and zircon U-Pb geochronology. However, Balagansky et al. (2015) and Shchipansky and Slabunov (2015) proposed that the obtained ca. 1.9 Ga zircon age in Kuru-Vaara eclogites is related to fluid infiltration during the Lapland-Kola collisional orogeny. The Paleoproterozoic ages obtained by garnet geochronology were debated as likely spuriously young ones created by resetting of the Sm-Nd and Lu-Hf systems (Balagansky et al., 2015; Dokukina and Mints, 2019; Li et al., 2015; Mints et al., 2014).

In our study, we provide evidence for eclogitization of the gabbro-norite dike (sample SG-38) thus defining a new eclogite type in the Kuru-Vaara quarry. We previously presented U-Pb zircon (Skublov et al., 2010, 2011b), as well as Sm-Nd (Mel'nik et al., 2013) and Lu-Hf (Herwartz et al., 2012) garnet ages for a concordant eclogite boudin (sample 46) from the Kuru-Vaara quarry and argued for a Paleoproterozoic age of the eclogite facies metamorphism. In this contribution, we provide detailed petrographic and mineralogical description for the eclogite that is based on study of sample SG-46/1 and new data on equivalent sample 46 from the same boudin. In contrast to sample 46, new U-Pb dating of eclogite SG-46/1 is based on a larger number of zircon grains that mainly contain mineral inclusions. Such an approach helps to better constrain and tie the zircon age to a particular stage in the rock history. Our novel data on garnet zoning from the eclogite boudin provide a framework for the new interpretation of the published Sm-Nd and Lu-Hf ages. In this paper, we additionally investigate trace element and oxygen isotope compositions of garnet and zircon in the eclogitic rocks in the Kuru-Vaara quarry to confirm the Paleoproterozoic age of eclogite facies metamorphism in the Belomorian Province.

2. Geological setting

The Belomorian Province is the polymetamorphic mobile belt located in the eastern part of the Fennoscandian Shield between the Karelian Craton and the Kola Province (Fig. 1a). This province records a long-lived evolution from Mesoarchean to Paleoproterozoic (Balagansky et al., 2015; Gaál and Gorbatschev, 1987; Glebovitsky et al., 1996; Slabunov et al., 2006), including poly-phase deformation at high- to moderate metamorphic grade from Neoarchean to Paleoproterozoic (Glebovitsky et al., 1996; Hölttä et al., 2008; Slabunov et al., 2006). The main constituents of the Belomorian Province are Archean greenstone complexes, TTG gneisses and paragneisses (Hölttä et al., 2008; Slabunov et al., 2006). The predominant ages of the protoliths of the TTG gneisses are in the range 2.93-2.72 Ga (Hölttä et al., 2008). The province belongs to the southwestern foreland of the Lapland-Kola collisional orogeny that occurred at 2.0-1.9 Ga (Mudruk et al., 2013).

Paleoproterozoic (2.5-1.9 Ga) plume-related mafic magmatism is widely presented in the eastern Fennoscandian Shield (Stepanova and Stepanov, 2010, and references therein) by volcanic rocks, dikes, and layered intrusions in the Karelian and Murmansk Cratons and Kola Province, and small intrusion and dikes in the Belomorian Province. Paleoproterozoic mafic dikes within the Belomorian Province are divided into three groups (Stepanova and Stepanov, 2010): 1) undated early Mg-tholeiitic dikes; 2) dikes of high-Mg gabbro-norites; 3) dikes of ca. 2.12 Fe-tholeiitic gabbro. These high-Mg gabbro-norites of the second group are related to the lherzolite-gabbronorite complex dated at 2.45-2.36 Ga (Lobach-Zhuchenko et al., 1998; Stepanova and Stepanov, 2010). A characteristic feature of all mafic rocks located in the Belomorian Province is the presence of coronitic textures resulted from metamorphism up to eclogite facies conditions (e.g., Perchuk and Morgunova, 2014; Stepanova and Stepanov, 2010; Travin, 2015).

Eclogite occurrences within the province are (Fig. 1a): Uzkaya Salma, Shirokaya Salma and Kuru-Vaara eclogites of the Salma area (e.g., Balagansky et al., 2015; Li et al., 2017a, 2017b, 2018;

Liu et al., 2017; Mel'nik et al., 2013; Mints et al., 2010, 2014; Skublov et al., 2011b); Gridino eclogites (e.g., Berezin et al., 2012; Dokukina and Mints, 2019; Dokukina et al., 2014; Li et al., 2015; Perchuk and Morgunova, 2014; Skublov et al., 2011a; Travin and Kozlova, 2009; Volodichev et al., 2004; Yu et al., 2019a); eclogites of the Keret Archipelago islands (Berezin et al., 2013; Berezin and Skublov, 2014; Skublov et al., 2016); the Krasnaya Guba eclogites (Kozlovskii and Aranovich, 2010; Kozlovsky and Aranovich, 2008; Skublov et al., 2013). Three adjacent locations (Kuru-Vaara quarry, Uzkaya Salma, and Shirokaya Salma) in the Salma area together with the Gridino complex (Fig. 1a) are the main eclogite-bearing occurrences within the province. They have a similar structure: a matrix of migmatized TTG gneiss contains boudin-like bodies of retrogressed eclogites (Li et al., 2017b, and references therein). The Gridino complex also includes numerous eclogitized gabbroic dikes (e.g., Dokukina and Mints, 2019; Perchuk and Morgunova, 2014; Yu et al., 2017). However, the metamorphosed gabbro-norite (this study) in the Kuru-Vaara quarry is the only eclogitized gabbroic rock reported for the Salma area. The magmatic age of the Gridino dikes has been regarded as either Archean (e.g., Dokukina and Mints, 2019) or Paleoproterozoic (e.g., Travin, 2015). The Archean magmatic age is based on the U-Pb dating of zircons, which could be trapped by the mafic dikes from the host TTG gneisses (Slabunov et al., 2011). The magmatic origin of the Gridino boudin-like eclogites is still debated. They have Archean magmatic protolith, which has been interpreted as representing either the former gabbroic dikes (e.g., Dokukina and Mints, 2019; Yu et al., 2017) or another protolith comparable with ophiolite mafic rocks (Volodichev et al., 2004). The protolith of boudin-like eclogite bodies from the Salma area has been attributed to Archean oceanic crust (e.g., Balagansky et al., 2015; Mints et al., 2014).

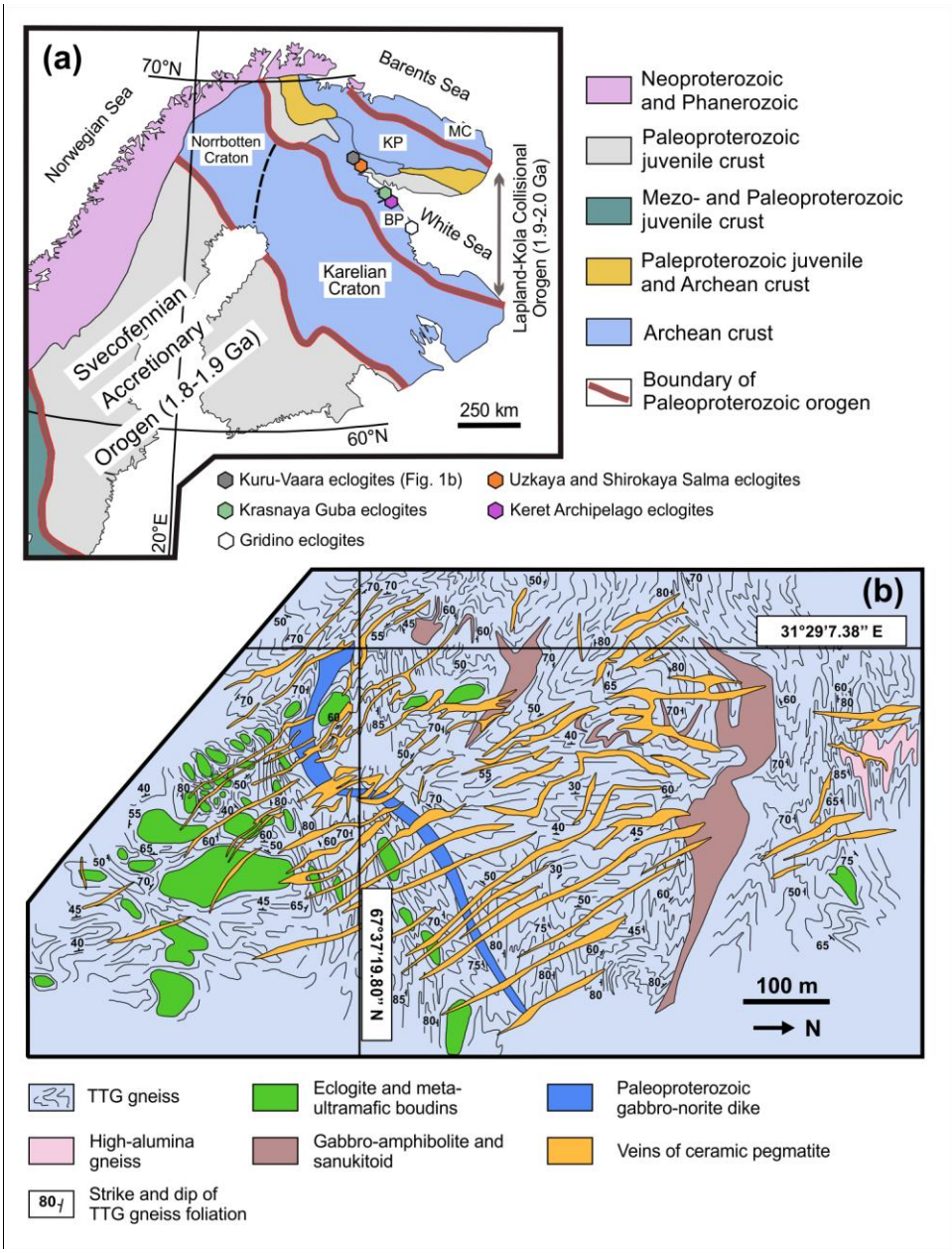

Figure 1. (a) Simplified geological map of the Fennoscandian Shield; BP, the Belomorian Province; KP, the Kola Province; MC, the Murmansk Craton (modified after Balagansky, 2002; Balagansky et al., 2015; Daly et al., 2006; Liu et al., 2017; Slabunov et al., 2006); (b) Geological map of the Kuru-Vaara quarry (modified after Liu et al., 2017; Shchipansky et al., 2012a).

The Kuru-Vaara quarry (Fig. 1b) exposes TTG gneiss (2.81 Ga, Shchipansky et al., 2012b) that hosts mafic and ultramafic boudins, a single dike of coronitic olivine gabbro-norite, bodies of Al-

rich gneiss, gabbro-amphibolite, sanukitoid, numerous pegmatites consisting mainly of quartz, feldspars, and mica (hereafter, ceramic pegmatite), and thin (up to 30 cm, Balagansky et al., 2015) corundum-bearing pegmatoid veins (not shown in the map). Detailed description of geology in the Kuru-Vaara quarry is presented in Balagansky et al. (2015) and Shchipansky et al. (2012a). The quarry contains two main eclogite types that are distinguished in petrography and structural position. (1) Eclogite boudins are deformed conformingly to the host TTG gneiss and vary in size from several meters to dozens of meters (Fig. 1b, Fig. 2a). (2) The partially eclogitized olivine gabbro-norite dike (Fig. 2b) that cuts across the structure of the TTG gneiss (Balagansky et al., 2015). This dike is slightly deformed, has a thickness of up to ~ 30 m and ~ 2 m chilled zones. Both eclogitic rock types underwent a single stage of retrogression (Balagansky et al., 2015; Liu et al., 2017; Shchipansky et al., 2012a). As a result, amphibolite facies assemblages partially or entirely replaced all eclogite facies assemblages (Fig. 2a). In accordance with petrography and position within the outcrop, the eclogite boudins were divided into two groups (the southern and the northern eclogites) by Shchipansky et al. (2012a). The corundum-bearing pegmatoid veins are attributed to amphibolite facies conditions and cross-cut the eclogite boudins (Balagansky et al., 2015; Liu et al., 2017). Veins of ceramic pegmatites cross-cut all the mentioned rocks in the quarry. U-Pb zircon dating yielded ages of 1885 ± 7 Ma (Liu et al., 2017) and 1841 ± 12 Ma (Skublov et al., 2011b) for the corundum-bearing pegmatoids and the ceramic pegmatites, respectively.

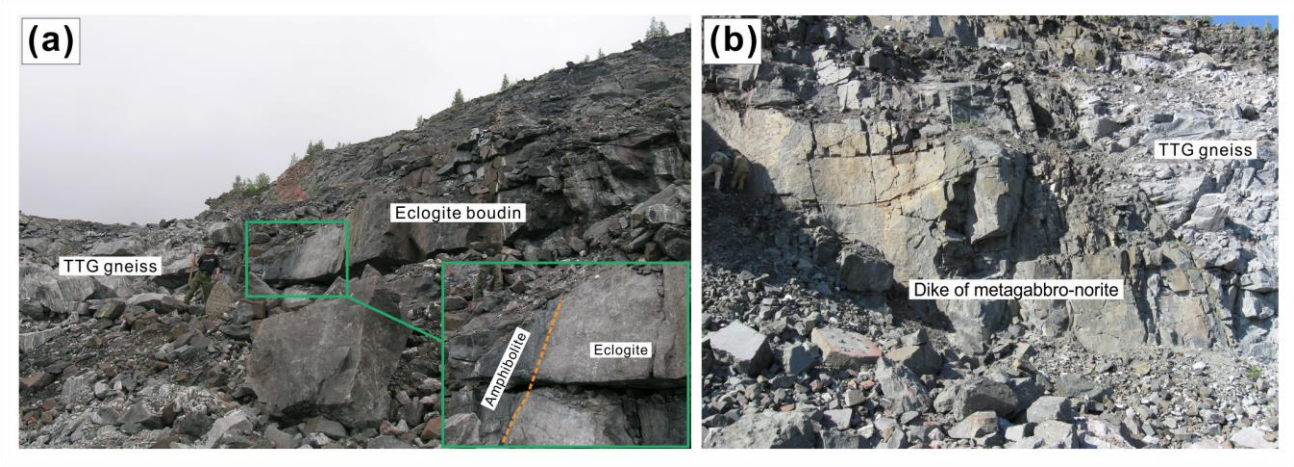

Figure 2. Field relationships between the eclogitic rocks and the host TTG gneisses in the Kuru-Vaara quarry. (a) An eclogite boudin (samples SG-46/1 and 46); the inset shows strong amphibolization of the eclogite boudin at the contact with gneisses. (b) The dated dike of an eclogitized olivine gabbro-norite (sample SG-38; SW-NE striking in Fig. 1b).

3. Analytical methods

3.1. Mineral characterization and major element composition

The major element composition of minerals was determined by scanning electron microscope equipped with an energy dispersive system (SEM-EDS) as well as by electron probe microanalysis (EPMA). SEM-EDS analyses were obtained at the Institute of Precambrian Geology and Geochronology of Russian Academy of Sciences using a scanning electron microscope JEOL JSM-6510 LA with an energy dispersive system JED-2200. The operating conditions were 20 kV accelerating voltage, a beam current of 1 nA, and a beam of 1-2 μm in diameter. Metals and natural minerals were used as standards. The data were corrected with the ZAF algorithm. EPMA measurements were conducted on a Cameca SX 100 at the Department for Earth and Environmental Sciences, LMU Munich, Germany. Analyses were done with an accelerating voltage of 15 keV, a current of 40 nA (10 nA for plagioclase analyses) and a focused beam. A dwell time of 10 seconds on the peak and 2x5 seconds on the two background positions was used for quantitative point analyses,

while qualitative compositional mappings were recorded with a dwell time of 250 ms/pixel at a step size of 5 μm/pixel. For garnet, pyroxene and amphibole, analyses for Si, Al, Fe and Mg were calibrated on almandine, while for plagioclase, Si and Al were calibrated on albite and Fe and Mg on almandine. For olivine, Si was calibrated on olivine, Al, Fe and Mg on almandine. For the other elements the following standards were used: wollastonite (Ca), albite (Na), orthoclase (K), ilmenite (Ti, Mn), vanadinite (Cl), Cr_2O_3 (Cr). Matrix correction was done by using the PAP ZAF routine, implemented in the Cameca PeakSight Software.

Garnet cations and end-members were calculated following the method of Locock (2008). Amphibole was calculated and classified according to Locock (2014) and Hawthorne et al. (2012), respectively. Pyroxene was classified according to Morimoto (1988).

Raman and photoluminescence (PL) micro-analyses of micro-inclusions in zircon were performed at Saint-Petersburg Mining University using a RenishawInVia Raman spectrometer. The analytical procedure and results are presented in the Supplementary material.

Mineral abbreviations are according to Whitney and Evans (2010).

3.2. Garnet and zircon trace element compositions

Measurements of trace elements in garnet and zircon were conducted at the Yaroslavl branch of the Institute of Physics and Technology of Russian Academy of Sciences (Yaroslavl, Russia) using a Cameca IMS-4f ion microprobe. Analytical procedures are mainly described in Batanova et al. (1998), Dokukina et al. (2014), Fedotova et al. (2008), Nosova et al. (2002), Portnyagin et al. (2008). For analysis, the primary O_2^- ion beam was focused to a spot size of ~20-25 μm. Each analysis was averaged from 3 cycles of measurements. Concentrations of trace elements were calculated from the normalized to $^{30}Si^+$ secondary ion intensities using calibration curves based on a set of reference glasses (Jochum et al., 2000, 2006). NIST-610 reference glass (Rocholl et al., 1997) was used as a

daily monitor for trace element analyses. Accuracy of the trace element measurements is up to 10% for concentrations higher than 1 ppm and up to 20% for the concentration range 0.1-1 ppm.

3.3. Oxygen isotopes in garnet

In situ oxygen isotopes analysis of garnet was performed by ion microprobe with a Cameca IMS 1280-HR at the SwissSIMS laboratory, University of Lausanne. Garnet was analyzed from polished individual grains and standard polished thin sections mounted together with primary and secondary garnet standards. Analytical conditions followed Seitz et al. (2017). A 10 kV Cs^+ primary Gaussian beam was used with a ~2.0 nA current, resulting in a spot size of ~15-20 μm. Analyses consisted of 20 cycles of 5 seconds each. Oxygen isotope ratios ($^{18}O/^{16}O$) are presented as deviations ($\delta^{18}O$) from the Vienna Standard Mean Ocean Water (VSMOW). UWG-2 garnet ($\delta^{18}O$ = 5.8‰, Valley et al, 1995) was used as a primary standard for instrumental mass fractionation. The in-house Umba garnet was run as a secondary standard and it returned $\delta^{18}O$ values standardized to UWG-2 without matrix correction of 15.2 ± 0.3‰ (2SD) over the session. This value is within uncertainty of the values obtained during sessions to calibrate the matrix bias correction scheme over the entire grossular range (Xgrs). As the analyzed garnet differs from standard UWG-2 in Xgrs of ~ 0.14-0.26, a matrix bias correction for grossular was applied according to the methods of Page et al. (2010) and Martin et al. (2014). The matrix correction equation used is bias = –3.32Grs2 + 8.31Grs – 1.08, where Grs is the molar fraction of grossular at the analyzed garnet spot based on SEM-EDS measurement (Table S1). The correction was based on the in-house reproduction of the Xgrs versus matrix bias curve obtained from 9 reference garnets as calculated in Vho et al. (2020). Since the difference in spessartine content between UWG-2 and the analyzed garnet is trivially small, a matrix bias correction for spessartine was not applied. No andradite correction was applied because small (Xadr of ~ 0.01-0.03 from EMPA data, Tables S2 and S5) or no measurable (SEM-EDS data, Table S1) andradite component is present in the investigated garnet, similarly to UWG-2 garnet. The uncertainty on the

final $\delta^{18}O$ for each analysis includes the internal error during analysis (2SE), the reproducibility on UWG-2 during the analytical session (0.27, 2SD) and the residual of the matrix correction (0.28, Vho et al., 2020).

3.4. Zircon U-Pb geochronology, oxygen isotopes

Zircon was separated using magnetic separation and heavy liquids. Handpicked zircon grains were embedded into epoxy resin together with reference zircon TEMORA 2 (Black et al., 2004) and 91500 (Wiedenbeck et al., 1995) and polished to expose their centers. To avoid influence of cracks and inclusions, we selected spots for in-situ analyses of zircon grains taking into account transmitted and reflected light images. Cathodoluminescence (CL) images were carried out on a Camscan MX2500S SEM equipped with a QLI/QUA2 CL detector at the Isotopic Investigation Centre of the All-Russian Geological Research Institute (St. Petersburg, Russia). Operating conditions for the SEM were 12 kV, a current of 5-7 nA and a working distance of 31-33 mm.

For sample SG-38, zircon U-Pb dating was carried out by a SHRIMP II ion microprobe at the Isotopic Investigation Centre of the All-Russian Geological Research Institute mainly following the analytical procedures described in Bröcker et al. (2014), Williams, (1998), Rodionov et al. (2012). The primary O_2^- oxygen beam (4 nA) was focused to a spot size of about 20 μm. U-Pb dating for zircon from sample SG-46/1 was conducted using a Cameca IMS-1280HR SIMS at the Institute of Geology and Geophysics, Chinese Academy of Sciences. The detailed analytical procedures were described by Li et al. (2009). The primary O_2^- ion beam had an intensity of ca. 6 nA, and a spot was about 20×30 μm in size. Positive secondary ions were extracted with a 10 kV potential. Cameca and SHRIMP analyses of the standard zircon TEMORA 2 were interspersed with unknown grains. Pb/U calibration was performed relative to zircon standard TEMORA 2 (417 Ma, Black et al., 2004). U and Th concentrations were calibrated against zircon standard 91500 (Wiedenbeck et al., 1995). For the Cameca IMS-1280HR analysis, a long-term uncertainty of 1.5% (1σ RSD) for $^{206}Pb/^{238}U$

measurements of the standard zircons was propagated to the unknowns (Li et al., 2010a). The analyses were corrected for common Pb on the basis of the measured ^{204}Pb assuming a common Pb composition according to the Stacey and Kramers (1975) model. Reduction of U-Pb data was performed with the use of the Isoplot/Ex program (Ludwig, 1999 and 2001).

Oxygen isotope compositions in zircon were obtained at the Institute of Geology and Geophysics of Chinese Academy of Sciences using Cameca IMS-1280 and Cameca IMS-1280HR ion microprobes. We followed analytical procedures similar to those described in Li et al. (2010b) and Tang et al. (2015). A primary Cs^+ beam (3-4 nA) was focused to a spot up to ~ 15 μm in size. The measured $^{18}O/^{16}O$ ratios were normalized to standard VSMOW ($^{18}O/^{16}O = 0.0020052$). We conducted measurements at the same analytical spots or close to those of U-Pb isotopes. Before measuring, samples were re-polished to remove pits of previous analyses. The instrumental mass fractionation (IMF) was corrected using TEMORA 2 reference zircon ($\delta^{18}O = 8.2‰$, Black et al., 2004). A second zircon standard 91500 was analyzed as an unknown to ascertain the veracity of the IMF. Eight (Cameca IMS-1280) and five (Cameca IMS-1280HR) measurements of 91500 zircon during the course of this study yield averages of $\delta^{18}O = 10.1 \pm 0.4$ and $10.1 \pm 0.7‰$ (2SD), respectively. That is consistent with the $\delta^{18}O$ value of 9.9‰ reported for 91500 zircon (Wiedenbeck et al., 2004). The uncertainty on a single $\delta^{18}O$ value includes the internal uncertainty (2SE) and the reproducibility on TEMORA 2 during the analytical sessions (2SD).

4. Petrography and mineral chemistry

4.1. Eclogite boudin (samples 46 and SG-46/1)

The two eclogite samples (Fig. 2a and S1) refer to “southern eclogites” of the Kuru-Vaara quarry according to definition of Shchipansky et al. (2012a). This rock is composed of garnet, amphibole, omphacite, diopside, plagioclase, quartz and minor rutile, kyanite, orthopyroxene, zoisite, apatite, zircon, and ilmenite. Preserved eclogite paragenesis comprises medium-grained (400-800 μm)

granoblastic omphacite, minor amphibole and kyanite, fine-grained quartz, rutile in the rock matrix, and coarse-grained (2-6 mm) garnet porphyroblasts. Partial retrogression of the eclogite is mainly reflected in amphibole + plagioclase kelyphitic coronas around garnet (Fig. 3a, c and 4a) and low-Na clinopyroxene + plagioclase ± amphibole symplectites replacing omphacite (Fig. 3a-c). The low-Na clinopyroxene is replaced by amphibole in the more altered parts of the rock. Retrograde sapphirine + spinel + plagioclase ± scapolite symplectites around medium-grained kyanite in the rock matrix have been reported by Liu et al. (2017) for an equivalent eclogite sample from the Kuru-Vaara quarry.

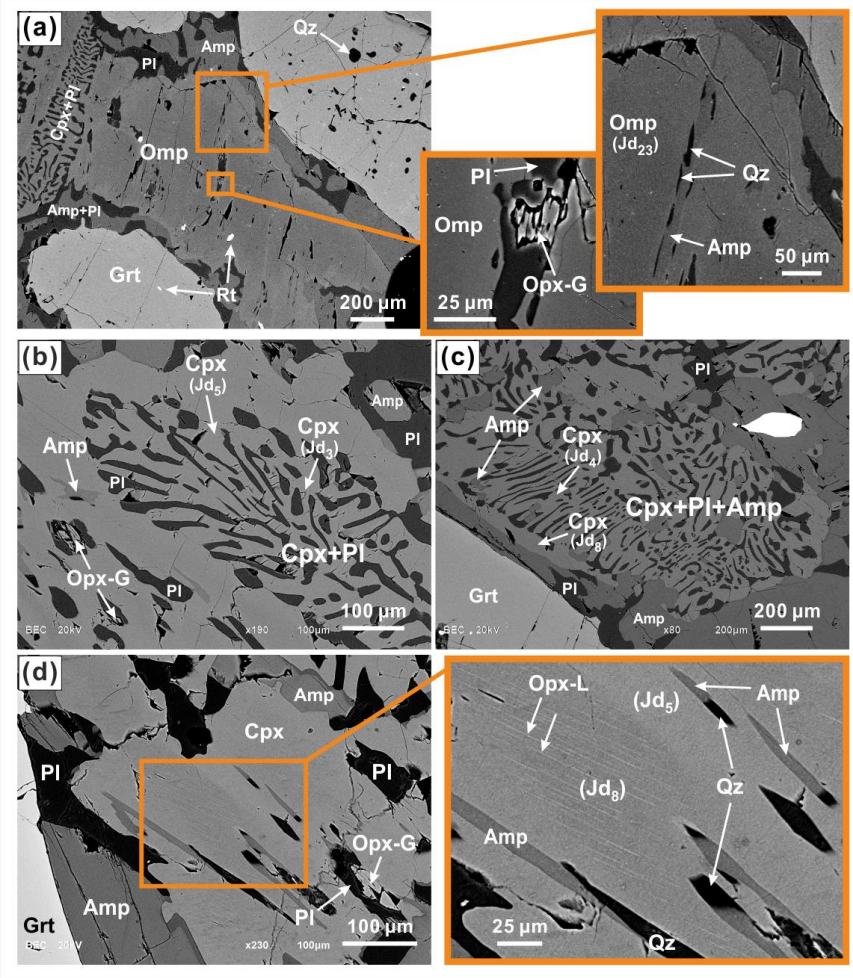

Figure 3. Back-scattered electron images of mineral textures in the eclogite boudin. (a) Partially retrogressed eclogite (sample 46). The insets show an orthopyroxene inclusion (Opx-G) with resorbed-like shape and quartz + amphibole rods within omphacite. (b) and (c) Diopside + plagioclase

and diopside + plagioclase + amphibole symplectites replacing omphacite, respectively (sample SG-46/1). (d) Fine orthopyroxene lamellae (Opx-L) in matrix diopside (sample SG-46/1). The lamellae are replaced by quartz + amphibole rods. The pyroxene jadeite content (mol.%) is reported in brackets.

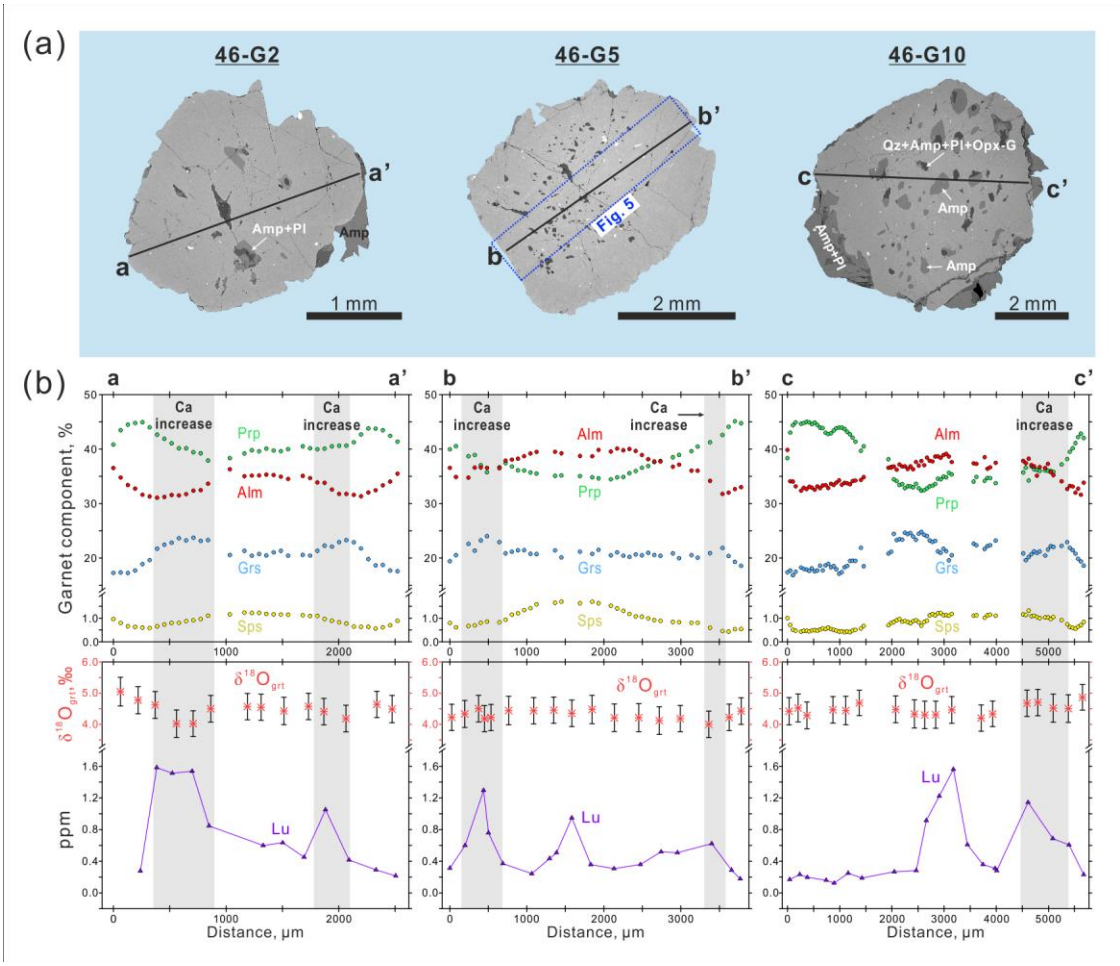

Figure 4. Zoned garnet grains of different sizes from the eclogite boudin (sample SG-46/1). (a) BSE images of the garnet grains with the marked profile along which mineral analyses were done. (b) Compositional (major elements, Lu and $\delta^{18}O$) cross-sections through the garnet grains. The grey bands show the approximate location of zones in garnet mantles with Ca increase. Error bars of $\delta^{18}O$ values are ± 2σ.

Garnet porphyroblasts are ellipsoidal and 2-6 mm in diameter. Mono- and poly-phase mineral inclusions of quartz, amphibole, plagioclase, rutile, diopside, orthopyroxene, ilmenite, and calcite have been observed in garnet. Previous studies (Konilov et al., 2011; Liu et al., 2017) reported also inclusions of kyanite, zoisite, and omphacite in garnet from equivalent samples of the "southern eclogites". In an attempt to better constrain garnet zoning, we carefully handpicked crystals of different size (2.5-6 mm, Fig. 4a) from sample SG-46/1, embedded them into separate epoxy mounts and polished every mount to expose the center of each crystal. Garnet has the following chemical compositions $Alm_{31\text{-}40}Prp_{32\text{-}45}Grs_{17\text{-}25}Sps_{0.4\text{-}1.7}$ and exhibits complex zonation (Fig. 4b and 5, Table S2). An increase of Mg and a decrease of Fe and Mn from core to rim is interpreted as preserved prograde growth zoning (e.g., Cheng et al., 2012). On the contrary, a decrease of Mg and an increase of Fe and Mn in the outermost 100-200 μm rim zone is attributed to retrograde diffusional zoning. All garnet grains have an increase of Ca concentration in an intermediate mantle zone (Fig. 4b), which is more notable in the compositional map (Fig. 5).

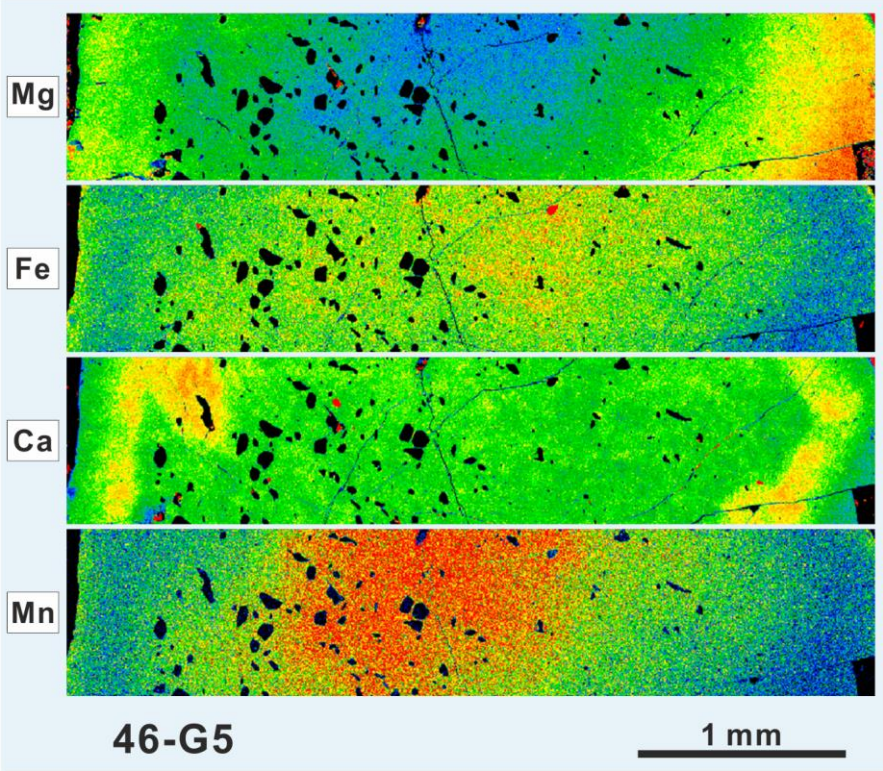

Figure 5. Mg, Fe, Ca and Mn X-ray maps of a portion of garnet grain 46-G5 from the eclogite boudin (sample SG-46/1). Blue color – low content; red color – high content. The mapped area is marked in Fig. 4a.

Garnet chondrite-normalized REE patterns display enrichment in HREE with respect to MREE and LREE (Fig. 6). The content of HREE is highest in the Ca-enriched mantle in all garnet grains and in the core of the largest grain (46-G10) (Fig. 4b and 6, Table S3). Generally, HREE contents decrease from the garnet center and rapidly rise in the Ca-rich mantle, to drop again in the outer rim (Fig. 4b and 6a-c).

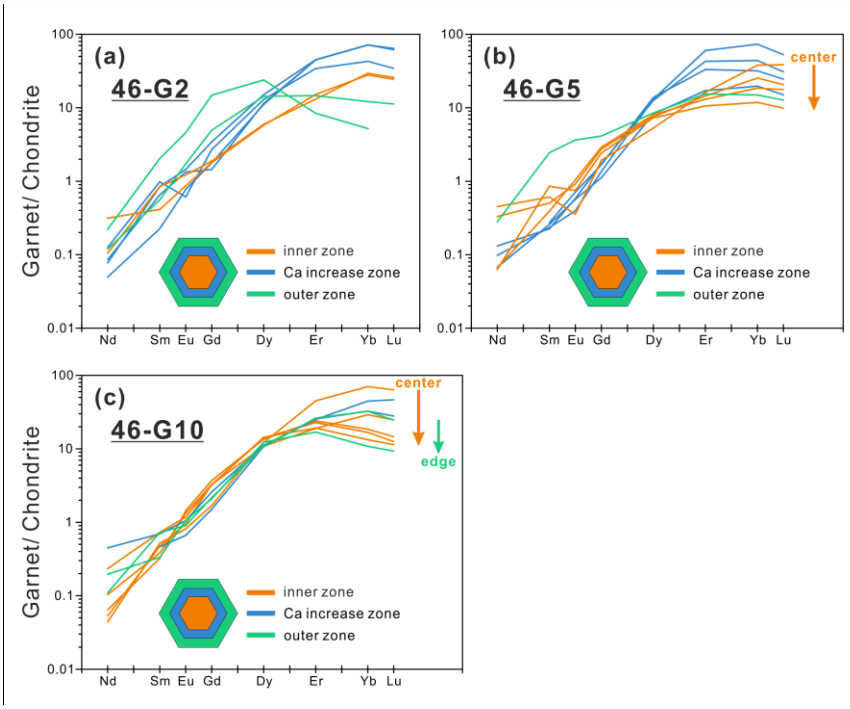

Figure 6. (a)-(c) Chondrite-normalized REE patterns for garnet from the eclogite boudin (sample SG-46/1). The garnet grains are shown in Fig. 4a. REE data are given for the center-to-edge section of every grain. REE concentrations were normalized using CI chondrite values (McDonough and Sun, 1995).

Medium-grained omphacite occurs in the matrix and includes orthopyroxene, quartz, amphibole, and rutile (Fig. 3a). Omphacite core contains 20-23 mol.% of jadeite component (Table S4), which decreases toward the rim (jadeite of 4-10 mol.%). This zoning is well visible in BSE images (Fig. 3a) and is likely related to re-equilibration during decompression. Either clinopyroxene + plagioclase or clinopyroxene + plagioclase + amphibole (Fig. 3b and c) symplectites usually replace the majority of omphacite grains. Clinopyroxene in the symplectites is diopside (jadeite content is 3-8 mol.%). Diopside inclusions in garnet have similar Na content (1-6 mol.% of jadeite component).

Amphibole in the eclogite has the following main occurrences: 1) magnesio-hornblende in the symplectites replacing omphacite (Fig. 3c); 2) pargasite and magnesio-hornblende in the coronas around garnet (Fig. 3a, c and 4a); 3) magnesio-hornblende in quartz + amphibole lamellae replacing

omphacite (Fig. 3a) and medium-grained matrix diopside (Fig. 3d); 4) pargasite and magnesio-hornblende inclusions in garnet (Fig. 4a); 5) matrix magnesio-hornblende in textural equilibrium with omphacite. Amphibole inclusions in garnet can be Cl-rich (up to 3.16 wt.%), while all other amphiboles are Cl-free (Table S4).

Andesine plagioclase (An_{37-42}) is found in the symplectites replacing omphacite and in the amphibole + plagioclase kelyphitic coronas around garnet. Plagioclase inclusions in garnet vary in composition from oligoclase to andesine (An_{25-48}, Table S4).

Orthopyroxene occurs as thin (< 1 μm) lamellae (Opx-L, Fig. 3d) exsolved from matrix diopside and as coarser (up to 100 μm) ubiquitous grains (Opx-G) with resorbed-like shape in garnet (Fig. 4a), in omphacite (Fig. 3a) and in the symplectites replacing omphacite (Fig. 3b and d). Opx-G as inclusion in omphacite and in the symplectites is always surrounded by plagioclase. Orthopyroxene inclusions in garnet are comparable in composition to matrix orthopyroxene (Al_2O_3 up to 1.86 wt.%, $En_{71-77}Fs_{23-28}$ and Al_2O_3 up to 1.99 wt.%, $En_{73-76}Fs_{23-26}$, respectively; Table S4).

4.2. Partially eclogitized dike (sample SG-38)

Coexistence of high-pressure (eclogitic) and magmatic mineral assemblages occurs in the more pristine portions of the metamorphosed olivine gabbro-norite dike (Fig. 2b and S1). The gabbro-norite has well-preserved medium- to coarse-grained (0.5-2 mm) cumulate and gabbroic textures; its magmatic assemblage is primarily composed of orthopyroxene, low-Na clinopyroxene, olivine, relics of Ca-rich plagioclase, minor biotite and ilmenite. The incomplete transformation from gabbro-norite to eclogite is indicated by coronitic and symplectitic textures reflecting partial/local equilibration during metamorphism.

In the olivine gabbro-norite from the Kuru-Vaara quarry, the eclogite facies assemblage occurs as complex coronas between magmatic orthopyroxene and plagioclase, which comprise sequential layers of omphacite, amphibole and garnet (Fig. 7a). The presence of the high-pressure mineral

assemblage besides magmatic relics is expressed with the terms "eclogitized" or "partially eclogitized" (John and Schenk, 2003; Korikovsky, 2005; Lang and Gilotti, 2001). Metamorphic coronas of omphacite-amphibole (around magmatic orthopyroxene) and orthopyroxene-amphibole-garnet or orthopyroxene-garnet (around olivine, Fig. 7b) are also common in sample SG-38. Sodic plagioclase + amphibole + spinel symplectites (Fig. 7) ubiquitously replace former magmatic Ca-rich plagioclase.

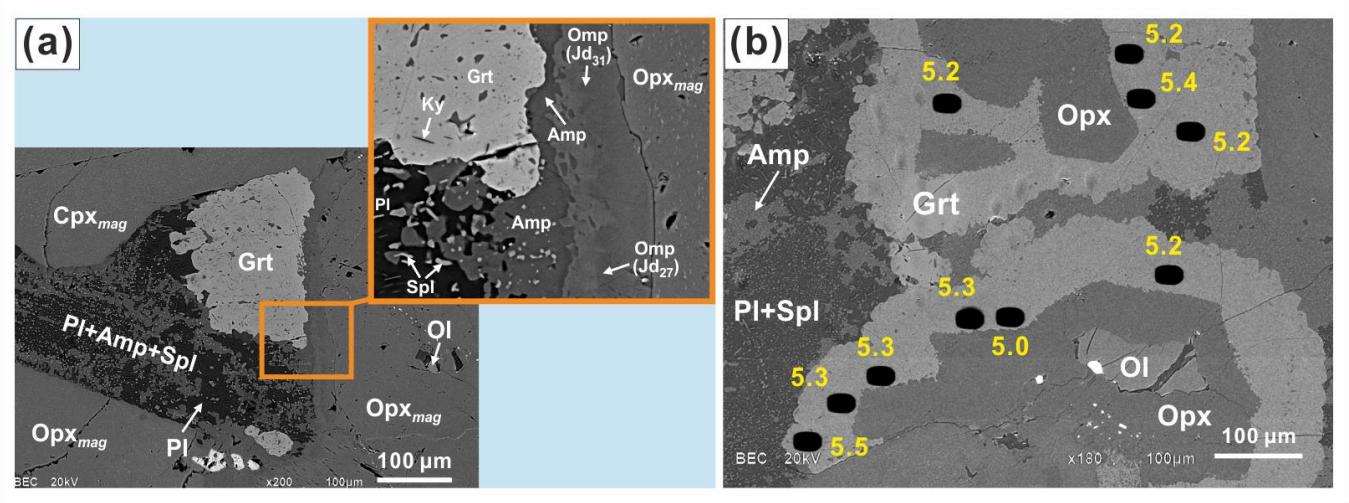

Figure 7. Back-scattered electron images of the eclogitized olivine gabbro-norite (sample SG-38). (a) Grt-Amp-Omp corona with eclogitic mineral assemblage around magmatic orthopyroxene; sodic Pl + Amp + Spl symplectites in a prior magmatic plagioclase domain. (b) Garnet-orthopyroxene corona around olivine and the symplectites in a prior magmatic plagioclase domain. The location of SIMS analyses of garnet (black pits) and corresponding $\delta^{18}O$ values in ‰ (yellow digits) are reported.

Representative chemical compositions of orthopyroxene, clinopyroxene, garnet, amphibole, plagioclase, and olivine are presented in Table S5. Magmatic orthopyroxene contains rare olivine inclusions and numerous tiny (<< 1 μm) exsolutions (Fig. 7a), identified as Cr-spinel (Balagansky et al., 2015). Compared with coronitic orthopyroxene, the magmatic one is enriched in Al_2O_3 (2.40-3.32

wt.%), Cr_2O_3 (0.35-1.15 wt.%), CaO (1.63-2.72 wt.%), and Na_2O (up to 0.31 wt.%). Cores of the magmatic orthopyroxene display the lowest Fe content, which is increasing towards the rims of the crystals (XFe = 0.13 and 0.18-0.20, respectively). The coronitic orthopyroxene is more Mg-rich (XMg = 0.80-0.85) than rim of the magmatic grains (XMg = 0.80-0.82).

Magmatic clinopyroxene is augite or diopside with a moderate jadeite content of 8-10 mol.% and contains tiny exsolutions of a Fe-rich phase. Omphacite composes the first layer of the complex coronas around magmatic orthopyroxene (Fig. 7a). The omphacite layer is relatively thin (10-30 μm) and compositionally heterogeneous with a high jadeite content of 21-31 mol.%. The highest jadeite content of this omphacite is comparable to the pyroxene composition in the eclogite boudins in the Kuru-Vaara quarry (29-33 mol.%, Liu et al., 2017; Shchipansky et al., 2012a).

Garnet occurs as an outer 100-150 μm layer in different coronas (Fig. 7a and b). Its composition is $Alm_{31-39}Prp_{39-48}Grs_{12-27}Sps_{1.2-1.7}$, comparable to that in the eclogite boudin. This garnet occurs within former magmatic plagioclase domains, and, in some cases, is intergrown with other minerals (mainly kyanite, amphibole, and sodic plagioclase), representing part of the breakdown assemblage of the magmatic plagioclase.

Amphiboles from coronas and from plagioclase domains have similar chemical compositions and represent pargasite. Preserved magmatic plagioclase is bytownite (Shchipansky et al., 2012a). In plagioclase + amphibole + spinel symplectites, the composition of the plagioclase varies from oligoclase to andesine (An_{19-43}). Spinel in the symplectites is Al-rich, but too small (<1-2 μm, Fig. 7a) to obtain reliable electron microprobe data. Matrix olivine has a high-Mg content (Fo_{79}).

5. Zircon geochronology, geochemistry and mineral inclusions

The U-Pb SIMS analyses for zircon are listed in Tables S6 and S7 and are shown in Figures 8 and S2. Corresponding trace element compositions are presented in Table S8.

Figure 8. CL images of representative zircon grains from the eclogite boudin (sample SG-46/1) and the partially eclogitized gabbro-norite (sample SG-38). Age (Ma ± 1σ; blue), Th/U ratio (black), oxygen isotope composition (green) and analysis number (orange) are labelled with different colors. The diameter of the orange circles is about 30 μm and the circle corresponds to the location of the SIMS analyses.

5.1. Eclogite boudin (sample SG-46/1)

The zircon grains recovered from the eclogite boudin are anhedral to subhedral crystals and

their fragments, isometric or elongated, usually colorless. Their size is up to 400 μm. The CL images revealed a complex structure of the zircon (Fig. 8 and S2). The most internal domain is a CL-dark or pale grey core that is observed in the majority of zircon crystals. The cores have variable shapes and commonly display weak oscillatory and/or sector zoning that is truncated by overgrowth domains. The zircon rim is composite and has a first zone with bright CL emission followed by one or several zones with darker CL emission. The CL-bright zone also forms the central part of those crystals that are free of the CL-dark cores. A few zircon grains without the CL-dark cores exhibit irregular or chaotic zoning patterns with medium to low CL emission. Core and rim analyses fall in two groups that define a Discordia line (Fig. 9a). Eleven U-Pb SIMS analyses of the cores are close to the upper intercept and yield an upper intercept age of 2907 ± 49 Ma. Three analyses constrain a Concordia age of 2884 ± 12 Ma, which is considered the most robust age of the zircon cores. The zircon cores have a high Th/U ratio of 0.81-3.28 (Tables S6). Chondrite-normalized patterns of the cores (Fig. 9c) show strong HREE enrichment (values of about 130-5700 times chondrite) with a positive pattern slope from Gd to Lu (Lu_N/Gd_N ratio = 9-18), distinct both negative Eu anomaly (Eu/Eu* = 0.06-0.14) and positive Ce anomaly (Ce/Ce* = 3.86-22.96). Ti-in-zircon thermometry (Watson et al., 2006) mainly yields temperatures of 810-1000°C for the zircon cores (Table S8). We did not identify primary mineral inclusions within these cores.

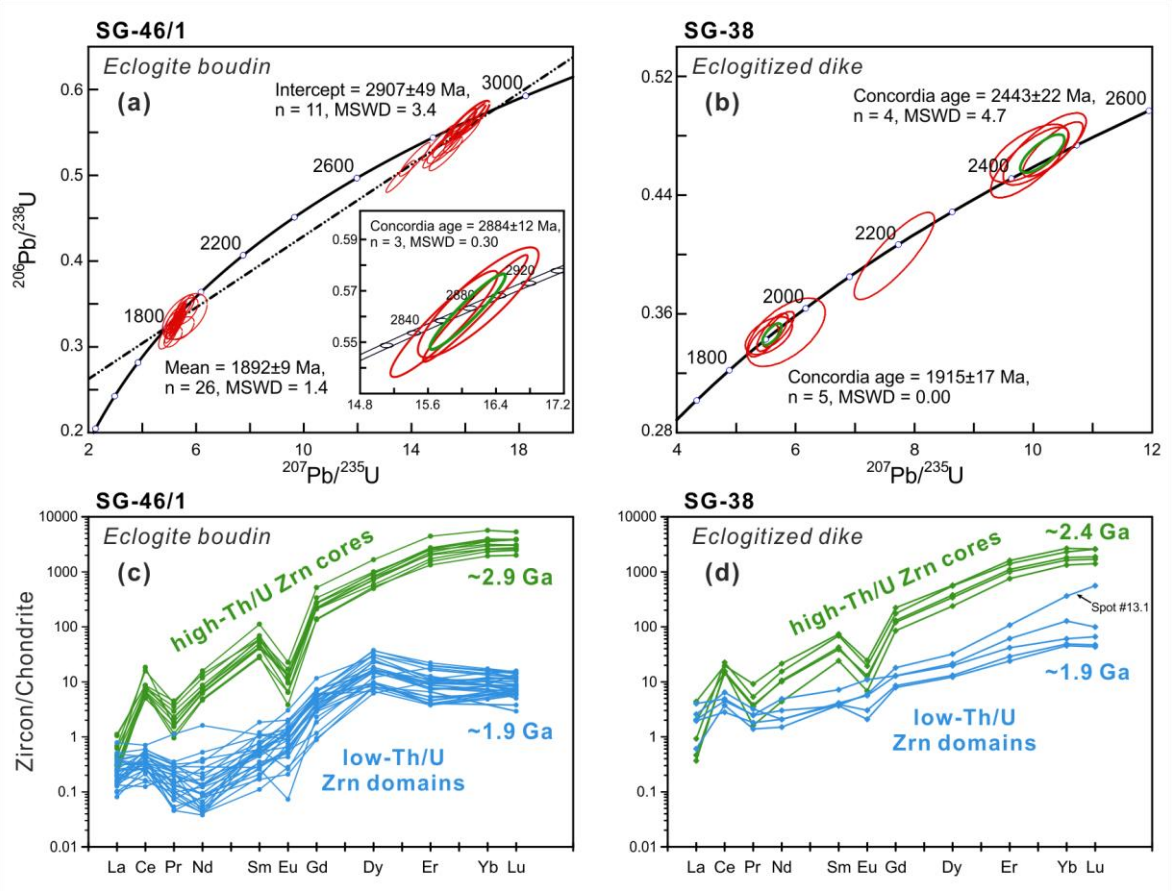

Figure 9. U-Pb concordia diagrams (a, b) and chondrite-normalized REE patterns (c, d) for zircon from the eclogite boudin (sample SG-46/1) and partially eclogitized gabbro-norite (sample SG-38). Error ellipses in the Concordia diagrams represent 2σ uncertainties. The Concordia ages, and the upper intercept and weighted average (mean) ages are given with 2σ and 95% confidence, respectively. REE data was normalized using CI chondrite values (McDonough and Sun, 1995).

In contrast to the zircon cores, all other domains of zircon grains display markedly low Th/U ratio of ≤ 0.06 (usually at the level of 0.00n-0.000n, Tables S6). The $^{207}Pb/^{206}Pb$ dates of the low-Th/U zircon domains are 2012-1833 Ma. Twenty-six U-Pb SIMS analyses of the low-Th/U zircon plot on or near Concordia, yielding a weighted average $^{207}Pb/^{206}Pb$ age of 1892 ± 9 Ma (Fig. 9a and S3). A few of the low-Th/U domains that are CL-bright have high common lead and very low U content, which did not allow to obtain correct U-Pb isotopic results (spots #11 and 34 in Table S6). Compared

to the cores, chondrite-normalized REE patterns of low-Th/U zircon domains display lower REE contents, especially HREE (values of about 1-38 times chondrite); HREE patterns are relatively flat (Lu_N/Gd_N ratio = 1-15, mainly 1-3), both Ce (Ce/Ce* = 0.75-3.97) and Eu (Eu/Eu* = 0.09-1.03, mainly 0.41-1.03) anomalies are minor (Fig. 9c). Ti-in-zircon thermometry (Watson et al., 2006) mainly yields temperatures of 620-700°C for the low-Th/U zircon (Table S8). The low-Th/U zircon domains exhibit individual and poly-phase mineral inclusions of zoisite, quartz, kyanite, garnet ($Alm_{40-49}Prp_{34-37}Grs_{14-21}Sps_{0.7-1.4}$), low-Na clinopyroxene (jadeite content of 7 mol.%), amphibole (pargasite), and plagioclase (An_{48}) (Fig. 8 and S2). One of the zircon grains is intergrown with plagioclase (An_{40}, Fig. 8). Inclusions of zoisite are predominant and can be associated with quartz, kyanite, and clinopyroxene. Compositions of representative garnet, amphibole, clinopyroxene, and plagioclase inclusions are listed in Table S9.

5.2. Partially eclogitized dike (sample SG-38)

Zircon grains separated from the eclogitized gabbro-norite are isometric and elongated (ca. 80-200 μm; Fig. 8 and S2). A notable zircon type in this sample is elongated aggregates of polygonal domains of 5-50 μm in size. Polygonal domains composing the aggregates display concentric zoning in CL images (Fig. 8).

Some elongated and isometric grains have oscillatory and sector zoned cores with a medium CL emission and irregular rims with homogeneous and bright in CL emission (up to 30 μm). The bright rims truncate the core zoning. One of the overgrowths contains a plagioclase (An_{40}) inclusion (Fig. S2). The $^{207}Pb/^{206}Pb$ ages of the oscillatory and sector zoned zircon cores are 2447-2218 Ma (Table S7); four analyses define a Concordia age of 2443 ± 22 Ma (Fig. 9b). The zoned zircon cores have a high Th/U ratio of 0.79-1.38 (Table S7). The REE patterns (Fig. 9d) show positive Ce anomaly (Ce/Ce* = 3.11-20.33) and negative Eu anomaly (Eu/Eu* = 0.15-0.19), HREE enrichment with a positive slope from Gd to Lu (Lu_N/Gd_N ratio = 11.7-16.6).

The prismatic zircon aggregates, a bright CL rim around one of the zoned cores, and a grain with a low CL emission all have $^{207}Pb/^{206}Pb$ ages in the range 1984-1891 Ma (Table S7); five analyses yield a Concordia age of 1915 ± 17 Ma (Fig. 9b). Compared with the zoned cores, this second zircon group shows low Th/U ratio of 0.02-0.27, mainly < 0.04 (Table S7). Chondrite-normalized REE patterns of the second zircon group display low REE contents and reduced Ce ($Ce/Ce^* = 1.49$-4.10) and Eu ($Eu/Eu^* = 0.39$-1.13) anomalies (Fig. 9d). Except for the zircon with low CL emission (spot #13.1), HREE patterns are relatively flat (Lu_N/Gd_N ratio = 5.2-7.7).

6. Garnet and zircon oxygen isotopes

Three garnet grains were analyzed for in-situ oxygen isotopes in sample SG-46/1 of the eclogite boudin. The $\delta^{18}O$ values for all grains are between 4.0-5.0‰ (grain G2 4.5 ± 0.6‰, grain G5 4.3 ± 0.3‰, grain G10 4.5 ± 0.3‰, total 4.4 ± 0.4‰, 2SD, n = 49) and particularly in grain G2 a weak zoning is observed (Fig. 4b, Table S10). This range of $\delta^{18}O$ is likely related to growth zoning over a T range in a constant bulk with variable assemblage (Korolev et al., 2018, and references therein). Similar oxygen isotope variations (about 1‰) were observed within growth-zoned garnets from other crustal eclogites (Russell et al., 2013). $\delta^{18}O$ values in the coronitic garnet of the eclogitized gabbro-norite are in a narrow range of 5.0-5.5‰ (5.3 ± 0.3‰, 2SD, n = 10; Fig. 7b, Table S10).

The oxygen isotopic SIMS analyses for the studied zircon are listed in Table S11 and shown in Figures 8 and S2. Values of $\delta^{18}O$ in the Archean zircon cores from the eclogite boudin (samples SG-46/1 and 46) are 5.1-5.9 ‰ (5.5 ± 0.5‰, 2SD, n = 13). The Paleoproterozoic low-Th/U zircon domains have lower $\delta^{18}O$ values of 4.5-5.4‰ (4.9 ± 0.5‰, 2SD, n = 33). The oscillatory and sector zoned zircon cores from the gabbro-norite dike (SG-38) display oxygen isotopes in a range of 5.2-5.7‰ (5.4 ± 0.4‰, 2SD, n = 5); oxygen isotope measurements for all other zircon domains yield $\delta^{18}O$ values of 4.7-5.7‰ (5.3 ± 0.8‰, 2SD, n = 4).

7. Discussion

7.1. Metamorphic history of Kuru-Vaara eclogites

Textural relationships and mineral compositions in the Kuru-Vaara eclogites can be reconciled with three metamorphic stages: (1) prograde, (2) eclogite facies metamorphic peak, and (3) retrogression.

(1) A prograde amphibolite facies conditions are inferred from numerous mineral inclusions of amphibole, diopside, plagioclase, quartz, rutile in prograde-zoned garnets from the eclogite boudin with Archean magmatic zircon ages. This stage probably involved Cl-bearing fluids as it can be inferred from Cl-enriched amphibole inclusions in garnet.

(2) Textural equilibrium of high-Mg garnet and high-Na clinopyroxene (omphacite) in the eclogite boudin and occurrence of these minerals in some metamorphic coronas around magmatic minerals of the partially eclogitized gabbro-norite constrain the peak metamorphic stage at eclogite facies. Rock-forming metamorphic minerals in coronitic and symplectitic textures of partially eclogitized gabbros usually reflect no evidence for long prograde growth, and their formation is mainly related to P-T conditions near the metamorphic peak (e.g., John and Schenk, 2003; Korikovsky, 2005; Perchuk and Morgunova, 2014). For this reason, the eclogitized dike exhibits no clear evidence for prograde metamorphism in contrast to the eclogite boudin. In previous studies (Balagansky et al., 2015; Shchipansky et al., 2012b, 2012a; Shchipansky and Slabunov, 2015), the appearance of the mineral coronas in the Kuru-Vaara gabbro-norite dike was ascribed to amphibolite facies metamorphism as the eclogite assemblage had not been identified. This can be explained by considering that omphacite may not uniformly spread in coronitic gabbro-norites since its occurrence depends on local rock chemistry (Korikovsky, 2005).

(3) The eclogite boudin exhibits evidence of overprinting retrogression. The observed tiny orthopyroxene lamellae in matrix diopside (Fig. 3d) can be interpreted as a result of omphacite breakdown at granulite facies overprint (Anderson and Moecher, 2007). Further, quartz-amphibole

rods replace these lamellae (Fig. 3d). The appearance of the rods in crustal eclogites occurs before the development of diopside + plagioclase ± amphibole symplectites (Anderson and Moecher, 2007). The retrograde granulite facies stage is firmly evident from sapphirine + spinel + plagioclase ± scapolite assemblage mantling the matrix kyanite in equivalent eclogites from the Kuru-Vaara quarry (Liu et al., 2017). Coarser orthopyroxene grains (Opx-G, Fig. 3b) in symplectites replacing omphacite were also ascribed to the granulite stage by Liu et al. (2017). However, Opx-G has a resorbed-like shape and can occur in omphacite and growth-zoned garnet. It allows assuming also inherited in addition to retrograde granulite nature for Opx-G. We speculate that at least some of the coarser orthopyroxene grains in the eclogite boudin could represent a former event in the rock history (e.g., inherited orthopyroxene of magmatic protolith). Our interpretation is supported by stability of orthopyroxene in high-Mg and high-Fe mafic rocks at eclogite grade conditions and further retrogression (e.g., Korikovsky, 2009; Nakamura, 2003). An example of magmatic orthopyroxene preservation through eclogite facies metamorphism and following strong retrogression is also provided by the retrogressed rock (Fig. S4) replacing the eclogitized gabbro-norite in the Kuru-Vaara quarry. After the granulite facies stage, Kuru-Vaara eclogites underwent amphibolite facies metamorphism, the initiation of which is testified by local amphibole growth after symplectitic diopside (Liu et al., 2017) and development of the kelyphitic coronas around garnet (Fig. 3a).

With the use of geothermobarometers, Shchipansky et al. (2012a) determined peak eclogite facies conditions of 12-14.5 kbar and 690-770°C for eclogite boudins in the Kuru-Vaara quarry. P-T conditions of peak eclogite facies and retrograde granulite facies stages were defined in Liu et al. (2017) as 18-20 kbar and 715-820°C, 11-13 kbar and 870-915°C, respectively. The further amphibolite facies overprint occurred at 5.3 kbar and 585°C (Balagansky et al., 2015).

7.2. Interpretation of zircon U-Pb ages

Zircon cores from both the eclogite boudin (sample SG-46/1) and partially eclogitized gabbro-norite (sample SG-38) exhibit common structural and geochemical signatures, such as oscillatory and sector zoning, HREE enrichment, distinct negative Eu and positive Ce anomalies, and high Th/U ratios. These signatures correspond to that of typical magmatic zircon (Belousova et al., 2002; Corfu et al., 2003; Grimes et al., 2015; Hoskin and Schaltegger, 2003; Rubatto, 2017) and thus we interpreted the zircon cores as dating the protolith crystallization. The eclogite boundin derives from a Mesoarchean protolith dated at 2884 ± 12 Ma. This is in line with or close to previously reported U-Pb zircon ages of 2929-2802 Ma and 2821 ± 24 Ma for the magmatic protolith of the southern eclogites of the Kuru-Vaara quarry (Liu et al., 2017; Shchipansky et al., 2012b). The protolith of the eclogitized gabbro-norite is constrained at 2443 ± 22 Ma. A U-Pb baddeleyite age of 2147 ± 28 Ma has been suggested as the gabbro-norite magmatic age by Balagansky et al. (2015). However, this age was obtained by analyzing both baddeleyite and metamorphic zircon overgrowth (see Fig. 10A and 10B in Balagansky et al., 2015). The obtained gabbro-norite zircon age of ca. 2.44 Ga corresponds to the formation of the lherzolite-gabbronorite complex dated at 2.45-2.36 Ga (Lobach-Zhuchenko et al., 1998; Stepanova and Stepanov, 2010), which includes numerous plume-induced intrusions (mainly dikes) that are widespread within the Belomorian Province. The Archean and Proterozoic magmatic zircon cores from both types of the Kuru-Vaara eclogites yield $\delta^{18}O$ values of 5.1-5.9‰ and 5.2-5.7‰, respectively. These values are consistent with the mantle zircon $\delta^{18}O$ value of 5.3 ± 0.3‰ (Valley et al., 2005), indicating crystallization from mantle-derived magmas for the eclogite protoliths.

The 1892 ± 9 Ma zircon rims and grains from the eclogite boudin exhibit low Th/U ratio and HREE depletion that are in line with growth of metamorphic zircon in equilibrium with garnet (Rubatto, 2002, 2017; Skublov et al., 2012). Their weak Eu anomaly can indicate absence or presence of only a small amount of plagioclase during zircon growth (e.g., Rubatto, 2002). In previous studies, these geochemical signatures were used to ascribe the Paleoproterozoic age of the zircon rims to eclogite facies metamorphism (sample 46 in Skublov et al., 2010, 2011b). Some additional insight

into the conditions of zircon formation comes from the mineral inclusions in the 1892 ± 9 Ma zircon domains. The most common mineral inclusion is zoisite, with minor kyanite, quartz, garnet, low-Na clinopyroxene (jadeite content of 7 mol.%), amphibole and plagioclase (An_{48}). According to our observations and previous studies (Liu et al., 2017; Shchipansky et al., 2012a; Skublov et al., 2011b), zoisite in the southern eclogites of the Kuru-Vaara quarry occurs only as inclusions in zircon and garnet, and is attributed to prograde metamorphism. To reconcile these data, we propose that the low Th/U zircon domains from the boudin eclogite (sample SG-46/1) formed during prograde metamorphism at 1892 ± 9 Ma. Based on thermodynamic calculations and the presence of inclusions of zoisite and kyanite in zircon, Liu at al. (2017) attributed formation of similar zircon domains dated at 1897-1895 Ma to the prograde metamorphism at eclogite facies conditions. However, coexistence of zoisite inclusions with kyanite and low-Na clinopyroxene (Jd_7) along with presence of plagioclase inclusion specify epidote-amphibolite/amphibolite but not eclogite facies conditions. Ti-in-zircon thermometry (Watson et al., 2006) mainly yields temperatures of 620-700°C for these zircons (Table S8), that are partly overlapping with the temperature estimates for prograde epidote-amphibolite facies metamorphism of Salma eclogites (610-660°C, Imayama et al., 2017; Yu et al., 2019b). The reported geochemical signature and mineral inclusion assemblage disagree with Balagansky et al. (2015) and Shchipansky and Slabunov (2015), who linked the ca. 1.9 Ga zircon with fluid infiltration during exhumation following the Lapland-Kola orogeny.

The 1915 ± 17 Ma zircon age group from the eclogitized gabbro-norite also has low-Th/U ratio and relative HREE depletion, in agreement with a metamorphic origin and simultaneous growth with garnet. Compared with the low Th/U zircon domains from the eclogite boudin, metamorphic zircon from the eclogitized gabbro-norite is distinguished by slightly higher HREE contents. The Paleoproterozoic ages of metamorphic zircon in both samples agree within error and are attributed to prograde metamorphism. The origin of the zircon aggregates (Fig. 8) from the gabbro-norite could be caused by their formation from baddeleyite (Corfu et al., 2003; Davidson and van Breemen, 1988)

during metamorphism as baddeleyite relics were found in the dike (Balagansky et al., 2015). Similar micro-zircon aggregates were also found in a high pressure metagabbro and interpreted as recrystallization of magmatic zircon by dissolution re-precipitation (Rubatto et al. 2008).

Ti-in-zircon thermometry (Table S8) and P-T pseudosections (Liu et al., 2017) constrain the growth of garnet and the ca. 1.9 Ga metamorphic zircon from the southern boudin eclogites to 600-800°C. Oxygen isotope fractionation between almandine garnet and zircon at 600-800 °C is <0.1‰ (Valley et al. 2003). Therefore, the $\delta^{18}O$ value of low Th/U zircon in the eclogite boudin supports growth of the Paleoproterozoic domains (4.9 ± 0.5‰) in equilibrium with garnet (4.4 ± 0.4‰,). The magmatic zircon cores yield instead a slightly higher $\delta^{18}O$ value (5.5 ± 0.5 ‰) and are not in oxygen isotopic equilibrium with garnet (Fig. 10). The slight decrease in zircon $\delta^{18}O$ between the magmatic and the metamorphic domains can be attributed to (i) oxygen isotope fractionation between minerals in different assemblages equilibrated at different temperatures (protoliths versus eclogite) or (ii) minor hydrothermal alteration of the protolith before or during metamorphism.

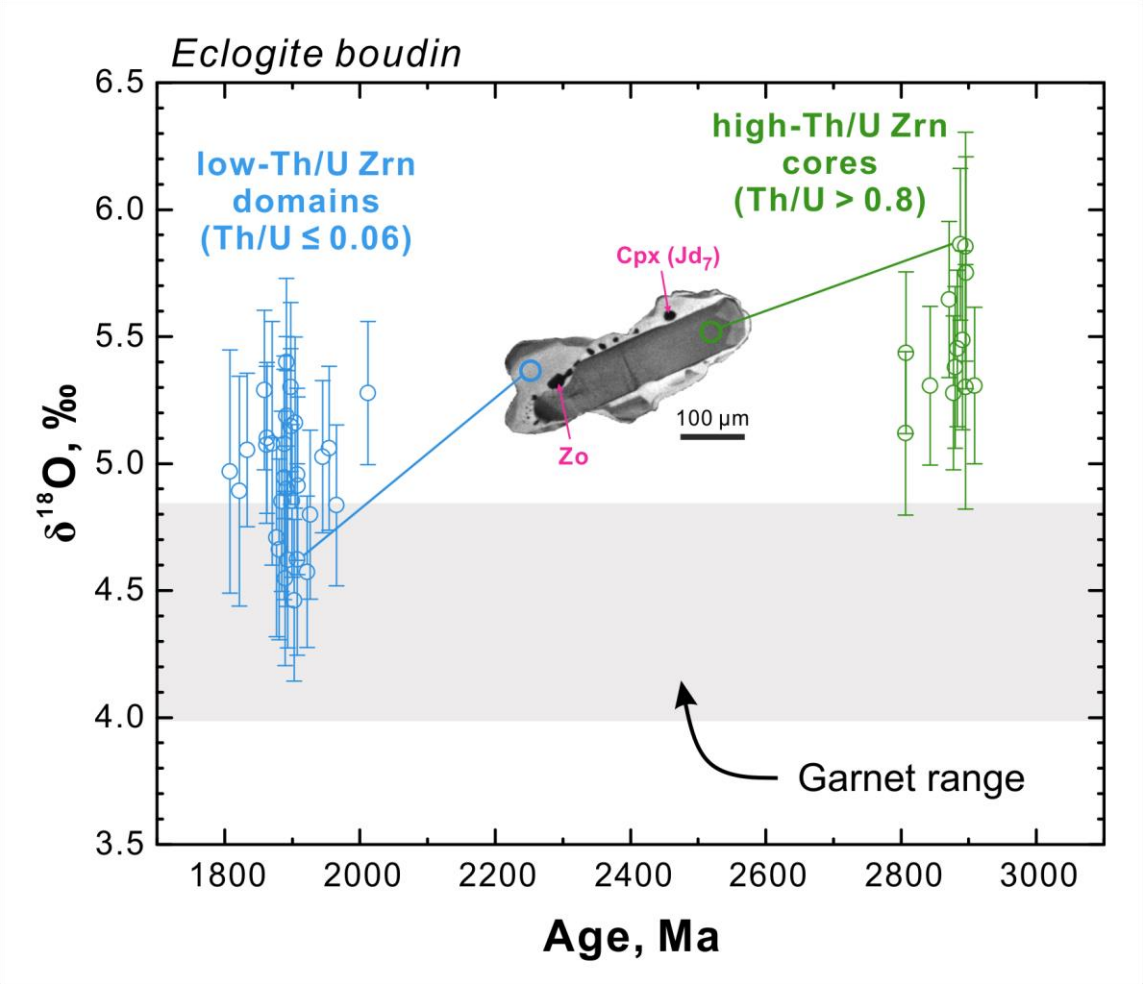

Figure 10. Zircon $\delta^{18}O$ values (‰ ± 2σ) versus $^{207}Pb/^{206}Pb$ ages (Ma) for the eclogite boudin (samples SG-46/1 and 46). The grey band represents an average $\delta^{18}O$ value of 4.4 ± 0.4‰ (2SD, n = 49) for garnet from the eclogite boudin. $^{207}Pb/^{206}Pb$ ages (Ma) for sample 46 (eight analyses) are after Skublov et al. (2010) (see Table S11).

In the eclogitized gabbro-norite, $\delta^{18}O$ values are comparable between the magmatic 2443 ± 22 Ma zircon (5.4 ± 0.4‰), metamorphic 1915 ± 17 Ma zircon (5.3 ± 0.8‰), and metamorphic garnet (5.3 ± 0.3‰). The constant oxygen isotope signature in magmatic and metamorphic minerals is in line with metamorphism of a rock relatively impermeable to externally derived fluids.

7.3. Petrological constraints on Sm-Nd and Lu-Hf ages

Sm-Nd and Lu-Hf garnet geochronology yields ages that can be linked with garnet growth if the closure temperatures are not exceeded. Ideally, the ages can be tied to a particular growth stage using major and trace element zoning of dated garnet (Cheng et al., 2008, 2011; Kelly et al., 2011; Lapen et al., 2003; Sandmann et al., 2016). Therefore, our new data on garnet zoning (sample SG-46/1) provide a framework for the re-interpretation of published ages for garnet from the same eclogite boudin (sample 46) in relation to specific metamorphic stages. Sample 46 has been dated to 1897 ± 16 Ma via Sm-Nd (Mel'nik et al., 2013) and to 1901 ± 5 Ma (Herwartz et al., 2012) via Lu-Hf. Both ages were previously attributed to eclogite facies metamorphism.

Garnet from the eclogite boudin (sample SG-46/1) shows primary bowl-shaped Mg and bell-shaped Fe and Mn patterns, which reflect that the initial growth zoning was unaffected or not totally erased by cation diffusion. The relatively sharp boundary of the Ca-rich mantle (Fig. 4 and 5) also supports preservation of growth zoning. The reverse Mg, Fe and Mn zoning in the garnet rim reflects instead marginal cation diffusion during the retrogression stage that overprinted the peak metamorphism. A high Lu concentration in the garnet core with decrease towards the rim is typical for HREE Rayleigh fractionation during garnet growth (e.g. Otamendi et al., 2002). In sample SG-46/1, the highest Lu concentrations correspond to garnet core and mantle. The general HREE increase in the mantle coincides with the Ca increase (Fig. 4b) and may be related to changes in mineral assemblages during the garnet growth. We propose that the growth of the Ca-enriched garnet mantle was accompanied by the consumption of Ca-rich minerals (zoisite and partly amphibole) as there are little primary amphibole and no zoisite in the rock matrix. Because omphacite inclusions have been observed in garnets from similar Kuru-Vaara eclogites (Konilov et al., 2011; Liu et al., 2017), and prograde eclogite grade stage where zoisite is stable has been proposed (Liu et al., 2017), the garnet mantle probably corresponds to zoisite consumption during the late prograde stage at eclogite facies conditions. Partial or complete diffusional re-equilibration of major elements in garnet while preserving Lu growth zoning indicates that the garnet Lu-Hf age has not been reset (Cheng et al.,

2008; Sandmann et al., 2016). Resetting of Lu-Hf system in garnets leads to Lu enrichment in garnet rims (Kelly et al., 2011; Kirchenbaur et al., 2012), which is not observed in the studied garnet from sample SG-46/1. Therefore, given a generally accepted high closure temperature of > 850-1000°C for the garnet Lu-Hf system (Scherer et al., 2000; Schmidt et al., 2011; Shu et al., 2014; Yu et al., 2019a), the maximum metamorphic temperature of ~900°C for the Kuru-Vara eclogites (Liu et al., 2017), and the preservation of growth zoning in Lu, the Lu-Hf garnet age is interpreted as the growth age.

A bulk Lu-Hf isochron age displays the average age of all growth zones in the dated garnet weighted by respective Lu abundances (Cheng et al., 2011). The studied garnet shows relative Lu enrichment in core (up to 1.6 ppm) and mantle (up to 1.6 ppm) portions. These portions correspond to separate episodes within a single prograde history of garnet growth. Therefore, the obtained Lu-Hf age of 1901 ± 5 Ma is taken to represent an average age of prograde garnet growth. Similar Paleoproterozoic Lu-Hf ages of 1.96-1.92 Ga have also been reported for the prograde stage of Gridino eclogites (Herwartz et al., 2012; Yu et al., 2019a). The obtained Sm-Nd age of 1897 ± 16 Ma is within uncertainty identical to the Lu-Hf prograde age. However, given the relatively lower closure temperature for the garnet Sm-Nd system (e.g., Scherer et al., 2000; Shu et al., 2014), and the considerable uncertainty, the Sm-Nd age of 1897 ± 16 Ma can reflect prograde to peak growth or cooling age of the dated garnet from the Kuru-Vaara eclogite.

7.4. A summary on eclogite ages

No evidence for Archean eclogite metamorphism has been found in this study. The eclogite metamorphism in the Kuru-Vaara must have happened after the youngest protolith intrusion at 2443 ± 22 Ma. Zircon U-Pb geochronology (1915 ± 17 and 1892 ± 9 Ma) and garnet Lu-Hf (1901 ± 5 Ma, Herwartz et al., 2012) isochron constrain the prograde stage. The corundum-bearing pegmatite veins in eclogite boudins and the ceramic pegmatites cross-cutting the eclogites post-date the eclogite metamorphism; these pegmatites formed at 1885-1841 Ma according to zircon U-Pb ages (Liu et al.,

2017; Skublov et al., 2011b). Comparable ca. 1.9 Ga ages were obtained for eclogite metamorphism by dating zircon with high pressure mineral inclusions (garnet and omphacite) from Gridino and Salma eclogites (Imayama et al., 2017; Yu et al., 2017). The Paleoproterozoic eclogite facies metamorphism in the Belomorian Province is linked with the Lapland-Kola collisional orogeny (e.g., Imayama et al., 2017; Li et al., 2017b; Yu et al., 2017).

8. Conclusions

1) The Kuru-Vaara quarry in the Belomorian Province exposes two main eclogite types: eclogite boudins and a partially eclogitized olivine gabbro-norite dike.

2) U-Pb dating of the magmatic zircon domains revealed Mesoarchean (2884 ± 12 Ma) and Paleoproterozoic (2443 ± 22 Ma) protolith ages for the eclogite boudin and the eclogitized gabbro-norite, respectively. The oxygen isotopic composition of the magmatic protolith zircon is in line with mantle-derived melts for both eclogite types.

3) The U-Pb age of zircon domains with metamorphic composition (REE and Th/U) in both eclogite types constrains prograde metamorphism for the Kuru-Vaara eclogites at 1915 ± 17 and 1892 ± 9 Ma. The mineral inclusion assemblage (garnet + zoisite + plagioclase + kyanite + amphibole + quartz + low-Na clinopyroxene) in the metamorphic zircon from the eclogite boudin provides evidence for epidote-amphibolite/amphibolite facies conditions of the prograde metamorphism.

4) Previously dated garnet in the boudin eclogite preserves trace element growth zoning with minor diffusion of major cations. The Paleoproterozoic Lu-Hf garnet age (1901 ± 5 Ma) can thus be robustly attributed to prograde metamorphism.

5) The oxygen isotopic composition of metamorphic zircon and garnet supports equilibrium between these two phases.

Acknowledgements

We thank Olga L. Galankina for collecting BSE images, Alice Vho for her invaluable help on evaluation of primary oxygen isotope data for garnet. We are grateful to Xiao-Xiao Ling, Guo-Qiang Tang, Jiao Li, and Yu Liu for help with U-Pb and oxygen isotopic analyses of zircon. We also thank Sergey G. Simakin and Evgeny V. Potapov for their help in conducting measurements of trace elements in garnet and zircon. The reported study was funded by the National Key R&D Program of China (grant 2016YFE0203000), the National Natural Science Foundation of China (grant 41811530083), and the Russian Foundation of Basic Research (RFBR), research projects № 18-55-53022 and 16-35-60092 mol_a_dk. This study was conducted under a state contract № 0153-2019-0002 (Institute of Precambrian Geology and Geochronology of Russian Academy of Sciences). A.E. Melnik acknowledges the awarding of a postdoctoral fellowship under the President's International Fellowship Initiative (PIFI) of the Chinese Academy of Sciences (grant 2019PC0100). D. Rubatto acknowledges the financial support of the Swiss National Science Foundation, project N. 200021_166280. We are thankful to Krishnan Sajeev and Volker Schenk for their very constructive comments and criticisms.

Supplementary material

Raman methods and results

Figure S1. View to the southwestern part of the Kuru-Vaara quarry with marked location of the studied eclogitized gabbro-norite dike (sample SG-38) and eclogite boudin (samples 46 and SG-46/1). White ellipses indicate approximate locations of sampling.

Figure S2. CL images of the additional zircon crystals that are not shown in Figure 8. Age (Ma ± 1σ; blue), Th/U ratio (black), oxygen isotope composition (green) and analysis number (orange) are labelled in different colors. Diameter of the orange and green circles is about 30 μm and the orange circles correspond to the location of the SIMS analyses. Green circles represent the location of the

oxygen isotopic and trace element analyses and are only shown where their location is different from the U-Pb analysis.

Figure S3. A weighted average $^{207}Pb/^{206}Pb$ age and individual $^{207}Pb/^{206}Pb$ age data for low-Th/U zircons from the eclogite boudin (sample SG-46/1). The weighted average age is given with 95% confidence. Error bars for individual data point are ± 2σ.

Figure S4. Back-scattered electron image for the retrogressed sample SG-38-A. The image shows the result of intense retrogression of the eclogitized gabbro-norite in the Kuru-Vaara quarry. Note the preserved protolith orthopyroxene despite eclogite facies metamorphism and subsequent retrogression.

Table S1. Garnet SEM-EDS data for matrix correction of oxygen isotopes.

Table S2. Electron microprobe data for garnet grains from sample SG-46/1 (see Fig. 4).

Table S3. Trace elements composition of garnet from sample SG-46/1 (SIMS data).

Table S4. Representative compositions of Cpx, Amp, Opx and Pl from samples 46* and SG-46/1 (SEM-EDS and EMP data).

Table S5. Representative compositions of Grt, Cpx, Amp, Opx, Pl and Ol from sample SG-38.

Table S6. Ion microprobe U-Pb (Cameca 1280-HR) data for zircon from sample SG-46/1.

Table S7. Ion microprobe U-Pb (SHRIMP-II) data for zircon from sample SG-38.

Table S8. Trace elements composition of zircon from samples SG-46/1 and SG-38 (SIMS data).

Table S9. Major elements composition of mineral inclusions in zircon from sample SG-46/1.

Table S10. Oxygen isotope analyses of garnet measured by ion microprobe.

Table S11. Oxygen isotope analyses of zircon measured by ion microprobe (Cameca 1280 for sample SG-46/1; Cameca 1280-HR for samples SG-38 and 46).

References

Abbott, D., Drury, R., Smith, W.H.F., 1994. Flat to steep transition in subduction style. Geology 22, 937–940. https://doi.org/10.1130/0091-7613(1994)022<0937:FTSTIS>2.3.CO;2

Anderson, E.D., Moecher, D.P., 2007. Omphacite breakdown reactions and relation to eclogite exhumation rates. Contrib. to Mineral. Petrol. 154, 253–277. https://doi.org/10.1007/s00410-007-0192-x

Balagansky, V.V., 2002. Main Stages of the Palaeoproterozoic Tectonic Evolution of the Northeastern Baltic Shield (Doctoral dissertation). Geological Institute of the Kola Science Center, Russian Academy of Sciences, Apatity, pp. 326 (in Russian).

Balagansky, V., Shchipansky, A., Slabunov, A.I., Gorbunov, I., Mudruk, S., Sidorov, M., Azimov, P., Egorova, S., Stepanova, A., Voloshin, A., 2015. Archaean Kuru-Vaara eclogites in the northern Belomorian Province, Fennoscandian Shield: Crustal architecture, timing, and tectonic implications. Int. Geol. Rev. 57, 1543–1565. https://doi.org/10.1080/00206814.2014.958578

Baldwin, J.A., Bowring, S.A., Williams, M.L., Williams, I.S., 2004. Eclogites of the Snowbird tectonic zone: Petrological and U-Pb geochronological evidence for Paleoproterozoic high-pressure metamorphism in the western Canadian Shield. Contrib. to Mineral. Petrol. 147, 528–548. https://doi.org/10.1007/s00410-004-0572-4

Batanova, V.G., Suhr, G., Sobolev, A. V., 1998. Origin of geochemical heterogeneity in the mantle peridotites from the Bay of Islands ophiolite, Newfoundland, Canada: Ion probe study of clinopyroxenes. Geochim. Cosmochim. Acta 62, 853–866. https://doi.org/10.1016/s0016-7037(97)00384-0

Belousova, E.A., Griffin, W.L., O'Reilly, S.Y., Fisher, N.I., 2002. Igneous zircon: Trace element composition as an indicator of source rock type. Contrib. to Mineral. Petrol. 143, 602–622. https://doi.org/10.1007/s00410-002-0364-7

Berezin, A.V., Skublov, S.G., Marin, Y.B., Mel'nik, A.E., Bogomolov, E.S., 2013. New occurrence

of eclogite in the Belomorian mobile belt: Geology, metamorphic conditions, and isotope age. Dokl. Earth Sci. 448. https://doi.org/10.1134/S1028334X13010029

Berezin, A. V., Skublov, S.G., 2014. Eclogite-like apogabbro rocks in Sidorov and Bolshaya Ileika islands, Keret Archipelago, White Sea: Compositional characteristics, metamorphic age and conditions. Petrology 22, 234–254. https://doi.org/10.1134/S0869591114030035

Berezin, A. V., Travin, V. V., Marin, Y.B., Skublov, S.G., Bogomolov, E.S., 2012. New U-Pb and Sm-Nd ages and P-T estimates for eclogitization in the Fe-Rich Gabbro Dyke in Gridino Area (Belomorian Mobile Belt). Dokl. Earth Sci. 444, 760–765. https://doi.org/10.1134/S1028334X12060207

Black, L.P., Kamo, S.L., Allen, C.M., Davis, D.W., Aleinikoff, J.N., Valley, J.W., Mundil, R., Campbell, I.H., Korsch, R.J., Williams, I.S., Foudoulis, C., 2004. Improved 206Pb/238U microprobe geochronology by the monitoring of a trace-element-related matrix effect; SHRIMP, ID-TIMS, ELA-ICP-MS and oxygen isotope documentation for a series of zircon standards. Chem. Geol. 205, 115–140. https://doi.org/10.1016/j.chemgeo.2004.01.003

Boniface, N., Schenk, V., Appel, P., 2012. Paleoproterozoic eclogites of MORB-type chemistry and three Proterozoic orogenic cycles in the Ubendian Belt (Tanzania): Evidence from monazite and zircon geochronology, and geochemistry. Precambrian Res. 192–195, 16–33. https://doi.org/10.1016/j.precamres.2011.10.007

Bröcker, M., Löwen, K., Rodionov, N., 2014. Unraveling protolith ages of meta-gabbros from Samos and the Attic-Cycladic Crystalline Belt, Greece: Results of a U-Pb zircon and Sr-Nd whole rock study. Lithos 198–199, 234–248. https://doi.org/10.1016/j.lithos.2014.03.029

Brown, M., 2014. The contribution of metamorphic petrology to understanding lithosphere evolution and geodynamics. Geosci. Front. 5, 553–569. https://doi.org/10.1016/j.gsf.2014.02.005

Brown, M., 2009. Metamorphic patterns in orogenic systems and the geological record. Geol. Soc.

Spec. Publ. 318, 37–74. https://doi.org/10.1144/SP318.2

Brown, M., 2008. Characteristic thermal regimes of plate tectonics and their metamorphic imprint throughout earth history: when did earth first adopt a plate tectonics mode of behavior? Spec. Pap. Geol. Soc. Am. 440, 97–128. https://doi.org/10.1130/2008.2440(05)

Brown, M., 2006. Duality of thermal regimes is the distinctive characteristics of plate tectonics since the Neoarchean. Geology 34, 961–964. https://doi.org/10.1130/G22853A.1

Cheng, H., King, R.L., Nakamura, E., Vervoort, J.D., Zhou, Z., 2008. Coupled Lu-Hf and Sm-Nd geochronology constrains garnet growth in ultra-high-pressure eclogites from the Dabie orogen. J. Metamorph. Geol. 26, 741–758. https://doi.org/10.1111/j.1525-1314.2008.00785.x

Cheng, H., Vervoort, J.D., Li, X., Zhang, C., Li, Q., Zheng, S., 2011. The growth interval of garnet in the UHP eclogites from the Dabie orogen, China. Am. Mineral. 96, 1300–1307. https://doi.org/10.2138/am.2011.3737

Cheng, H., Zhang, C., Vervoort, J.D., Lu, H., Wang, C., Cao, D., 2012. Zircon U-Pb and garnet Lu-Hf geochronology of eclogites from the Lhasa Block, Tibet. Lithos 155, 341–359. https://doi.org/10.1016/j.lithos.2012.09.011

Collins, A.S., Reddy, S.M., Buchan, C., Mruma, A., 2004. Temporal constraints on Palaeoproterozoic eclogite formation and exhumation (Usagaran Orogen, Tanzania). Earth Planet. Sci. Lett. 224, 175–192. https://doi.org/10.1016/j.epsl.2004.04.027

Condie, K.C., & Kröner, A., 2008. When did plate tectonics begin? Evidence from the geologic record. The Geological Society of America, Special Paper 440, 281–294.

Corfu, F., Hanchar, J.M., Hoskin, P.W.O., Kinny, P., 2003. Atlas of zircon textures. Rev. Mineral. Geochemistry 53, 469–500. https://doi.org/10.2113/0530469

Daly, J.S., Balagansky, V. V., Timmerman, M.J., Whitehouse, M.J., 2006. The Lapland-Kola orogen: Palaeoproterozoic collision and accretion of the northern Fennoscandian lithosphere. Geol. Soc. Mem. 32, 579–598. https://doi.org/10.1144/GSL.MEM.2006.032.01.35

Davidson, A., van Breemen, O., 1988. Baddeleyite-zircon relationships in coronitic metagabbro, Grenville Province, Ontario: implications for geochronology. Contrib. to Mineral. Petrol. 100, 291–299. https://doi.org/10.1007/BF00379740

Dokukina, K., Mints, M., 2019. Subduction of the Mesoarchaean spreading ridge and related metamorphism, magmatism and deformation by the example of the Gridino eclogitized mafic dyke swarm, the Belomorian Eclogite Province, eastern Fennoscandian Shield. J. Geodyn. 123, 1–37. https://doi.org/10.1016/j.jog.2018.11.003

Dokukina, K.A., Kaulina, T. V., Konilov, A.N., Mints, M. V., Van, K. V., Natapov, L., Belousova, E., Simakin, S.G., Lepekhina, E.N., 2014. Archaean to Palaeoproterozoic high-grade evolution of the Belomorian eclogite province in the Gridino area, Fennoscandian Shield: Geochronological evidence. Gondwana Res. 25, 585–613. https://doi.org/10.1016/j.gr.2013.02.014

Fedotova, A.A., Bibikova, E. V., Simakin, S.G., 2008. Ion-microprobe zircon geochemistry as an indicator of mineral genesis during geochronological studies. Geochemistry Int. 46, 912-927. https://doi.org/10.1134/S001670290809005X

François, C., Debaille, V., Paquette, J.L., Baudet, D., Javaux, E.J., 2018. The earliest evidence for modern-style plate tectonics recorded by HP–LT metamorphism in the Paleoproterozoic of the Democratic Republic of the Congo. Sci. Rep. 8, 15452. https://doi.org/10.1038/s41598-018-33823-y

Gaál, G., Gorbatschev, R., 1987. An outline of the Precambrian evolution of the Baltic Shield. Precambrian Res. 35, 15-52. https://doi.org/10.1016/0301-9268(87)90044-1

Glebovitsky, V.A., Miller, Y.V., Drugova, G.M., Milkevich, R.I., and Vrevskii, A.B., 1996, The structure and metamorphism of the Belomoride–Lapland collision zone. Geotectonics 30, 53–63.

Grimes, C.B., Wooden, J.L., Cheadle, M.J., John, B.E., 2015. “Fingerprinting” tectono-magmatic

provenance using trace elements in igneous zircon. Contrib. to Mineral. Petrol. 170, 1–26. https://doi.org/10.1007/s00410-015-1199-3

Hawthorne, F.C., Oberti, R., Harlow, G.E., Maresch, W. V., Martin, R.F., Schumacher, J.C., Welch, M.D., 2012. Ima report: Nomenclature of the amphibole supergroup. Am. Mineral. 97, 2031–2048. https://doi.org/10.2138/am.2012.4276

Herwartz, D., Skublov, S.G., Berezin, A. V., Mel'nik, A.E., 2012. First Lu-Hf garnet ages of eclogites from the Belomorian Mobile Belt (Baltic Shield, Russia). Dokl. Earth Sci. 443, 377–380. https://doi.org/10.1134/s1028334x12030130

Hölttä, P., Balagansky, V., Garde, A.A., Mertanen, S., Peltonen, P., Slabunov, A., Sorjonen-Ward, P., Whitehouse, M., 2008. Archean of Greenland and Fennoscandia. Episodes 31, 13–19. https://doi.org/10.18814/epiiugs/2008/v31i1/003

Hoskin, P.W.O., Schaltegger, U., 2003. The composition of zircon and igneous and metamorphic petrogenesis. Rev. Mineral. Geochemistry 53, 27–62.

Imayama, T., Oh, C.W., Baltybaev, S.K., Park, C.S., Yi, K., Jung, H., 2017. Paleoproterozoic high-pressure metamorphic history of the Salma eclogite on the Kola Peninsula, Russia. Lithosphere 9, 855–873. https://doi.org/10.1130/L657.1

Jochum, K.P., Dingwell, D.B., Rocholl, A., Stoll, B., Hofmann, A.W., Becker, S., Besmehn, A., Besserte, D., Dietze, H.J., Dulski, P., Erzinger, J., Hellebrand, E., Hoppe, P., Horn, I., Janssens, K., Jenner, G.A., Klein, M., McDonough, W.F., Maetz, M., Mezger, K., Münker, C., Nikogosian, I.K., Pickhardt, C., Raczek, I., Rhede, D., Seufert, H.M., Simakin, S.G., Sobolev, A. V., Spettel, B., Straub, S., Vincze, L., Wallianos, A., Weckwerth, G., Weyer, S., Wolf, D., Zimmer, M., 2000. The preparation and preliminary characterisation of eight geological MPI-DING reference glasses for in-situ microanalysis. Geostand. Newsl. 24, 87–133. https://doi.org/10.1111/j.1751-908X.2000.tb00590.x

Jochum, K.P., Stoll, B., Herwig, K., Willbold, M., Hofmiann, A.W., Amini, M., Aarburg, S.,

Abouchami, W., Hellebrand, E., Mocek, B., Raczek, I., Stracke, A., Alard, O., Bouman, C., Becker, S., Dücking, M., Brätz, H., Klemd, R., De Bruin, D., Canil, D., Cornell, D., De Hoog, C.J., Dalpé, C., Danyushevshy, L., Eisenhauer, A., Gao, Y., Snow, J.E., Groschopf, N., Günther, D., Latkoczy, C., Guillong, M., Hauri, E.H., Höfer, H.E., Lahaye, Y., Horz, K., Jacob, D.E., Kasemann, S.A., Kent, A.J.R., Ludwig, T., Zack, T., Mason, P.R.D., Meixner, A., Rosner, M., Misawa, K., Nash, B.P., Pfänder, J., Premo, W.R., Sun, W.D., Tiepolo, M., Vannucci, R., Vennemann, T., Wayne, D., Woodhead, J.D., 2006. MPI-DING reference glasses for in situ microanalysis: New reference values for element concentrations and isotope ratios. Geochemistry, Geophys. Geosystems 7, Q02008. https://doi.org/10.1029/2005GC001060

John, T., Schenk, V., 2003. Partial eclogitisation of gabbroic rocks in a late Precambrian subduction zone (Zambia): Prograde metamorphism triggered by fluid infiltration. Contrib. to Mineral. Petrol. 146, 174–191. https://doi.org/10.1007/s00410-003-0492-8

Kelly, E.D., Carlson, W.D., Connelly, J.N., 2011. Implications of garnet resorption for the Lu-Hf garnet geochronometer: An example from the contact aureole of the Makhavinekh Lake Pluton, Labrador. J. Metamorph. Geol. 29, 901–916. https://doi.org/10.1111/j.1525-1314.2011.00946.x

Kirchenbaur, M., Pleuger, J., Jahn-Awe, S., Nagel, T.J., Froitzheim, N., Fonseca, R.O.C., Münker, C., 2012. Timing of high-pressure metamorphic events in the Bulgarian Rhodopes from Lu-Hf garnet geochronology. Contrib. to Mineral. Petrol. 163, 897–921. https://doi.org/10.1007/s00410-011-0705-5

Konilov, A.N., Shchipansky, A.A., Mints, M. V., Dokukina, K.A., Kaulina, T. V., Bayanova, T.B., Natapov, L.M., Belousova, E.A., Griffin, W.L., O'Reilly, S.Y., 2011. The Salma Eclogites of the Belomorian Province, Russia: HP/UHP Metamorphism Through the Subduction of Mesoarchean Oceanic Crust, Ultrahigh-Pressure Metamorphism. In: Dobrzhinetskaya, L., Cuthbert, S., Faryad, W., Wallis, S. (Eds.), Ultrahigh-Pressure Metamorphism: 25 Years after the Discovery of Coesite and Diamond. Elsevier, 623–670 (Chapter 19).

https://doi.org/10.1016/B978-0-12-385144-4.00018-7

Korikovsky, S.P., 2005. Prograde transformations of gabbronorites during eclogitization in the temperature range 600-700 °C. Russ. Geol. Geophys. 46, 1352-1366.

Korikovsky, S.P., 2009. Prograde transformations of medium-pressure amphibolites during their eclogitization. Petrology 17, 315–330. https://doi.org/10.1134/S0869591109040018

Korolev, N.M., Melnik, A.E., Li, X.-H., Skublov, S.G., 2018. The oxygen isotope composition of mantle eclogites as a proxy of their origin and evolution: A review. Earth-Science Rev. 185, 288-300. https://doi.org/10.1016/j.earscirev.2018.06.007

Kozlovskii, V.M., Aranovich, L.Y., 2010. Petrology and thermobarometry of eclogite rocks in the Krasnaya Guba dike field, Belomorian Mobile Belt. Petrology 18, 27–49. https://doi.org/10.1134/S0869591110010029

Kozlovsky, V.M., Aranovich, L.Y., 2008. Geological and structural conditions of eclogitization of Paleoproterozoic basic dikes in the eastern Belomorian Mobile Belt. Geotectonics 42, 305–317. https://doi.org/10.1134/S0016852108040043

Lang, H.M., Gilotti, J.A., 2001. Plagioclase replacement textures in partially eclogitised gabbros from the Sanddal mafic-ultramafic complex, Greenland Caledonides. J. Metamorph. Geol. 19, 495–515. https://doi.org/10.1046/j.0263-4929.2001.00325.x

Lapen, T.J., Johnson, C.M., Baumgartner, L.P., Mahlen, N.J., Beard, B.L., Amato, J.M., 2003. Burial rates during prograde metamorphism of an ultra-high-pressure terrane: An example from Lago di Cignana, western Alps, Italy. Earth Planet. Sci. Lett. 215, 57–72. https://doi.org/10.1016/S0012-821X(03)00455-2

Li, Q.L., Li, X.H., Liu, Y., Tang, G.Q., Yang, J.H., Zhu, W.G., 2010a. Precise U-Pb and Pb-Pb dating of Phanerozoic baddeleyite by SIMS with oxygen flooding technique. J. Anal. At. Spectrom. 25, 1107–1113. https://doi.org/10.1039/b923444f

Li, X., Yu, H., Zhang, L., Wei, C., Bader, T., 2017a. 1.9 Ga eclogite from the Archean-

Paleoproterozoic Belomorian Province, Russia. Sci. Bull. 62, 239–241. https://doi.org/10.1016/j.scib.2017.01.026

Li, X., Zhang, L., Wei, C., Slabunov, A.I., 2015. Metamorphic PT path and zircon U-Pb dating of Archean eclogite association in Gridino complex, Belomorian province, Russia. Precambrian Res. 268, 74–96. https://doi.org/10.1016/j.precamres.2015.07.009

Li, X., Zhang, L., Wei, C., Slabunov, A.I., Bader, T., 2018. Quartz and orthopyroxene exsolution lamellae in clinopyroxene and the metamorphic P–T path of Belomorian eclogites. J. Metamorph. Geol. 36, 1–22. https://doi.org/10.1111/jmg.12280

Li, X., Zhang, L., Wei, C., Slabunov, A.I., Bader, T., 2017b. Neoarchean-Paleoproterozoic granulite-facies metamorphism in Uzkaya Salma eclogite-bearing mélange, Belomorian Province (Russia). Precambrian Res. 294, 257–283. https://doi.org/10.1016/j.precamres.2017.03.031

Li, X.H., Liu, Y., Li, Q.L., Guo, C.H., Chamberlain, K.R., 2009. Precise determination of Phanerozoic zircon Pb/Pb age by multicollector SIMS without external standardization. Geochemistry, Geophys. Geosystems 10, 1–21. https://doi.org/10.1029/2009GC002400

Li, X.H., Long, W.G., Li, Q.L., Liu, Y., Zheng, Y.F., Yang, Y.H., Chamberlain, K.R., Wan, D.F., Guo, C.H., Wang, X.C., Tao, H., 2010b. Penglai Zircon Megacrysts: A Potential New Working Reference Material for Microbeam Determination of Hf-O Isotopes and U-Pb Age. Geostand. Geoanalytical Res. 34, 117–134. https://doi.org/10.1111/j.1751-908X.2010.00036.x

Liu, F., Zhang, L., Li, X., Slabunov, A.I., Wei, C., Bader, T., 2017. The metamorphic evolution of Paleoproterozoic eclogites in Kuru-Vaara, northern Belomorian Province, Russia: Constraints from P-T pseudosections and zircon dating. Precambrian Res. 289, 31–47. https://doi.org/10.1016/j.precamres.2016.11.011

Lobach-Zhuchenko, S.B., Arestova, N.A., Chekulaev, V.P., Levsky, L.K., Bogomolov, E.S., Krylov, I.N., 1998. Geochemistry and petrology of 2.40-2.45 Ga magmatic rocks in the north-

western Belomorian Belt, Fennoscandian Shield, Russia. Precambrian Res. 92, 223–250. https://doi.org/10.1016/S0301-9268(98)00076-X

Locock, A.J., 2014. An Excel spreadsheet to classify chemical analyses of amphiboles following the IMA 2012 recommendations. Comput. Geosci. 62, 1–11. https://doi.org/10.1016/j.cageo.2013.09.011

Locock, A.J., 2008. An Excel spreadsheet to recast analyses of garnet into end-member components, and a synopsis of the crystal chemistry of natural silicate garnets. Comput. Geosci. 34, 1769–1780. https://doi.org/10.1016/j.cageo.2007.12.013

Loose, D., Schenk, V., 2018. 2 . 09 Ga old eclogites in the Eburnian-Transamazonian orogen of southern Cameroon : Significance for Palaeoproterozoic plate tectonics Precambr. Res. 304, 1–11. https://doi.org/10.1016/j.precamres.2017.10.018

Ludwig, K.R., 1999. User's Manual for Isoplot/Ex, Version 2.10. A GeochronologicalToolkit for Microsoft Excel. Berkeley Geochronology Center Special Publication, 1.

Ludwig, K.R., 2001. Users manual for Isoplot/Ex (Rev. 2.49). Berkeley Geochronology Center Special Publication, 1, 55.

Martin, L.A.J., Rubatto, D., Crépisson, C., Hermann, J., Putlitz, B., Vitale-Brovarone, A., 2014. Garnet oxygen analysis by SHRIMP-SI: Matrix corrections and application to high-pressure metasomatic rocks from Alpine Corsica. Chem. Geol. 374–375, 25–36. https://doi.org/10.1016/j.chemgeo.2014.02.010

McDonough, W.F., Sun, S. s., 1995. The composition of the Earth. Chem. Geol. 120, 223–253. https://doi.org/10.1016/0009-2541(94)00140-4

Mel'nik, A.E., Skublov, S.G., Marin, Y.B., Berezin, A.V., Bogomolov, E.S., 2013. New data on the age (U-Pb, Sm-Nd) of garnetites from Salma eclogites of the Belomorian mobile belt. Dokl. Earth Sci. 448, 78-85. https://doi.org/10.1134/S1028334X13010133

Mints, M. V., Belousova, E.A., Konilov, A.N., Natapov, L.M., Shchipansky, A.A., Griffin, W.L.,

O'Reilly, S.Y., Dokukina, K.A., Kaulina, T. V., 2010. Mesoarchean subduction processes: 2.87 Ga eclogites from the Kola Peninsula, Russia. Geology 38, 739–742. https://doi.org/10.1130/G31219.1

Mints, M.V., Dokukina, K.A., 2020. Age of eclogites formed by the subduction of the Mesoarchaean oceanic crust (Salma, Belomorian Eclogite Province, eastern Fennoscandian Shield, Russia): A synthesis. Precambr. Res. 350, 105879 https://doi.org/10.1016/j.precamres.2020.105879.

Mints, M. V., Dokukina, K.A., Konilov, A.N., 2014. The Meso-Neoarchaean Belomorian eclogite province: Tectonic position and geodynamic evolution. Gondwana Res. 25, 561–584. https://doi.org/10.1016/j.gr.2012.11.010

Möller, A., Appel, P., Mezger, K., Schenk, V., 1995. Evidence for a 2 Ga subduction zone: eclogites in the Usagaran belt of Tanzania. Geology 23, 1067–1070. https://doi.org/10.1130/0091-7613(1995)023<1067:EFAGSZ>2.3.CO;2

Morimoto, N., 1988. Nomenclature of Pyroxenes. Mineral. Petrol. 39, 55–76. https://doi.org/10.1007/BF01226262

Mudruk, S.V., Balagansky, V.V., Gorbunov, I.A., Raevsky, A.B., 2013. Alpine-type tectonics in the Paleoproterozoic Lapland-Kola Orogen. Geotectonics 47, 251–265. https://doi.org/10.1134/S0016852113040055

Müller, S., Dziggel, A., Sindern, S., Kokfelt, T.F., Gerdes, A., Kolb, J., 2018. Age and temperature-time evolution of retrogressed eclogite-facies rocks in the Paleoproterozoic Nagssugtoqidian Orogen, South-East Greenland: Constrained from U-Pb dating of zircon, monazite, titanite and rutile. Precambrian Res. 314, 468–486. https://doi.org/10.1016/j.precamres.2018.07.002

Nakamura, D., 2003. Stability of phengite and biotite in eclogites and characteristics of biotite- or orthopyroxene-bearing eclogites. Contrib. to Mineral. Petrol. 145, 550–567. https://doi.org/10.1007/s00410-003-0469-7

Nosova, A.A., Sazonova, L. V., Narkisova, V. V., Simakin, S.G., 2002. Minor elements in clinopyroxene from paleozoic volcanics of the Tagil island arc in the Central Urals. Geochemistry Int. 40, 219–232.

Otamendi, J.E., de la Rosa, J.D., Patino Douce, A.E., Castro, A., 2002. Rayleigh fractionation of heavy rare earths and yttrium during metamorphic garnet growth. Geology 30, 159–162. https://doi.org/10.1130/0091-7613(2002)030<0159:RFOHRE>2.0.CO;2

Page, F.Z., Kita, N.T., Valley, J.W., 2010. Ion microprobe analysis of oxygen isotopes in garnets of complex chemistry. Chem. Geol. 270, 9–19. https://doi.org/10.1016/j.chemgeo.2009.11.001

Perchuk, A.L., Morgunova, A.A., 2014. Variable P-T paths and HP-UHP metamorphism in a Precambrian terrane, Gridino, Russia: Petrological evidence and geodynamic implications. Gondwana Res. 25, 614–629. https://doi.org/10.1016/j.gr.2012.09.009

Portnyagin, M., Almeev, R., Matveev, S., Holtz, F., 2008. Experimental evidence for rapid water exchange between melt inclusions in olivine and host magma. Earth Planet. Sci. Lett. 272, 541–552. https://doi.org/10.1016/j.epsl.2008.05.020

Rocholl, A.B.E., Simon, K., Jochum, K.P., Bruhn, F., Gehann, R., Kramar, U., Luecke, W., Molzahn, M., Pernicka, E., Seufert, M., Spettel, B., Stummeier, J., 1997. Chemical characterisation of NIST silicate glass certified reference material SRM 610 by ICP-MS, TIMS, LIMS, SSMS, INAA, AAS and PIXE. Geostand. Newsl. 21, 101–114. https://doi.org/10.1111/j.1751-908X.1997.tb00537.x

Rodionov, N. V., Belyatsky, B. V., Antonov, A. V., Kapitonov, I.N., Sergeev, S.A., 2012. Comparative in-situ U-Th-Pb geochronology and trace element composition of baddeleyite and low-U zircon from carbonatites of the Palaeozoic Kovdor alkaline-ultramafic complex, Kola Peninsula, Russia. Gondwana Res. 21, 728–744. https://doi.org/10.1016/j.gr.2011.10.005

Rubatto, D., 2017. Zircon: The Metamorphic Mineral. Rev. Mineral. Geochemistry 83, 261–295. https://doi.org/10.2138/rmg.2017.83.09

Rubatto, D., 2002. Zircon trace element geochemistry: Partitioning with garnet and the link between U-Pb ages and metamorphism. Chem. Geol. 184, 123–138. https://doi.org/10.1016/S0009-2541(01)00355-2

Rubatto, D., Müntener, O., Barnhoorn, A., Gregory, C., 2008. Dissolution-reprecipitation of zircon at low-temperature, high-pressure conditions (Lanzo Massif, Italy). Am. Mineral. 93, 1519–1529. https://doi.org/10.2138/am.2008.2874

Russell, A.K., Kitajima, K., Strickland, A., Medaris, L.G., Schulze, D.J., Valley, J.W., 2013. Eclogite-facies fluid infiltration: Constraints from δ18O zoning in garnet. Contrib. to Mineral. Petrol. 165, 103–116. https://doi.org/10.1007/s00410-012-0794-9

Sandmann, S., Herwartz, D., Kirst, F., Froitzheim, N., Nagel, T.J., Fonseca, R.O.C., Münker, C., Janák, M., 2016. Timing of eclogite-facies metamorphism of mafic and ultramafic rocks from the Pohorje Mountains (Eastern Alps, Slovenia) based on Lu–Hf garnet geochronometry. Lithos 262, 576–585. https://doi.org/10.1016/j.lithos.2016.08.002

Scherer, E.E., Cameron, K.L., Blichert-Toft, J., 2000. Lu-Hf garnet geochronology: Closure temperature relative to the Sm-Nd system and the effects of trace mineral inclusions. Geochim. Cosmochim. Acta 64, 3413-3432. https://doi.org/10.1016/S0016-7037(00)00440-3

Schmidt, A., Mezger, K., O'Brien, P.J., 2011. The time of eclogite formation in the ultrahigh pressure rocks of the Sulu terrane. Constraints from Lu-Hf garnet geochronology. Lithos 125, 743–756. https://doi.org/10.1016/j.lithos.2011.04.004

Seitz, S., Baumgartner, L.P., Bouvier, A.S., Putlitz, B., Vennemann, T., 2017. Quartz Reference Materials for Oxygen Isotope Analysis by SIMS. Geostand. Geoanalytical Res. 41, 69–75. https://doi.org/10.1111/ggr.12133

Shchipansky, A.A., Khodorevskaya, L.I., Konilov, A.N., Slabunov, A.I., 2012a. Eclogites from the Belomorian Mobile Belt (Kola Peninsula): Geology and petrology. Russ. Geol. Geophys. 53, 1–21. https://doi.org/10.1016/j.rgg.2011.12.001

Shchipansky, A.A., Khodorevskaya, L.I., Slabunov, A.I., 2012b. The geochemistry and isotopic age of eclogites from the Belomorian Belt (Kola Peninsula): Evidence for subducted Archean oceanic crust. Russ. Geol. Geophys. 53, 262–280. https://doi.org/10.1016/j.rgg.2012.02.004

Shchipansky, A.A., Slabunov, A.I., 2015. Provenance of "Svecofennian" zircons in the Belomorian mobile belt, Baltic shield, and some geodynamic implications. Geochemistry Int. 53, 869–891. https://doi.org/10.1134/S0016702915100043

Shu, Q., Brey, G.P., Gerdes, A., Hoefer, H.E., 2014. Mantle eclogites and garnet pyroxenites - the meaning of two-point isochrons, Sm-Nd and Lu-Hf closure temperatures and the cooling of the subcratonic mantle. Earth Planet. Sci. Lett. 389, 143–154. https://doi.org/10.1016/j.epsl.2013.12.028

Sizova, E., Gerya, T., Brown, M., Perchuk, L.L., 2010. Subduction styles in the Precambrian: Insight from numerical experiments. Lithos 116, 209–229. https://doi.org/10.1016/j.lithos.2009.05.028

Skublov, S.G., Astaf'ev, B.Y., Marin, Y.B., Berezin, A.V., Mel'nik, A.E., Presnyakov, S.L., 2011a. New data on the age of eclogites from the Belomorian mobile belt at Gridino settlement area. Dokl. Earth Sci. 439, 1163-1170. https://doi.org/10.1134/S1028334X11080290

Skublov, S.G., Balashov, Y.A., Marin, Y.B., Berezin, A. V., Mel'nik, A.E., Paderin, I.P., 2010. U-Pb age and geochemistry of zircons from Salma eclogites (Kuru-Vaara deposit, Belomorian Belt). Dokl. Earth Sci. 432, 791–798. https://doi.org/10.1134/s1028334x10060188

Skublov, S.G., Berezin, A.V., Melnik, A.E., Astafiev, B.Y., Voinova, O.A., Alekseev, V.I., 2016. Protolith age of eclogites from the southern part of Pezhostrov Island, Belomorian belt: Protolith of metabasites as indicator of eclogitization time. Petrology 24, 594-607. https://doi.org/10.1134/S0869591116040056

Skublov, S.G., Berezin, A. V., Berezhnaya, N.G., 2012. General relations in the trace-element composition of zircons from eclogites with implications for the age of eclogites in the

belomorian mobile belt. Petrology 20, 427–449. https://doi.org/10.1134/S0869591112050062

Skublov, S.G., Berezin, A.V., Mel'nik, A.E., 2011b. Paleoproterozoic eclogites in the salma area, Northwestern Belomorian Mobile Belt: Composition and isotopic geochronologic characteristics of minerals and metamorphic age. Petrology 19, 470–495. https://doi.org/10.1134/S0869591111050055

Skublov, S.G., Mel'nik, A.E., Marin, Y.B., Berezin, A.V., Bogomolov, E.S., Ishmurzin, F.I., 2013. New data on the age (U-Pb, Sm-Nd) of metamorphism and a protolith of eclogite-like rocks from the Krasnaya Guba Area, Belomorian Belt. Dokl. Earth Sci. 453. https://doi.org/10.1134/S1028334X13110184

Slabunov, A.I., Volodichev, O.I., Skublov, S.G., Berezin, A. V., 2011. Main stages of the formation of paleoproterozoic eclogitized gabbro-norite: Evidence from U-Pb (SHRIMP) dating of zircons and study of their genesis. Dokl. Earth Sci. 437, 396–400. https://doi.org/10.1134/S1028334X11030202

Slabunov, A.I., Lobach-Zhuchenko, S.B., Bibikova, E. V., Balagansky, V. V., Sorjonen-Ward, P., Volodichev, O.I., Shchipansky, A.A., Svetov, S.A., Chekulaev, V.P., Arestova, N.A., Stepanov, V.S., 2006. The Archean of the Baltic Shield: Geology, geochronology, and geodynamic settings. Geotectonics 40, 409–433. https://doi.org/10.1134/S001685210606001X

Stacey, J.S., Kramers, J.D., 1975. Approximation of terrestrial lead isotope evolution by a two-stage model. Earth Planet. Sci. Lett. 26, 207-221. https://doi.org/10.1016/0012-821X(75)90088-6

Stepanova, A., Stepanov, V., 2010. Paleoproterozoic mafic dyke swarms of the Belomorian Province, eastern Fennoscandian Shield. Precambrian Res. 183, 602–616. https://doi.org/10.1016/j.precamres.2010.08.016

Tang, G.Q., Li, X.H., Li, Q.L., Liu, Y., Ling, X.X., Yin, Q.Z., 2015. Deciphering the physical mechanism of the topography effect for oxygen isotope measurements using a Cameca IMS-1280 SIMS. J. Anal. At. Spectrom. 30, 950–956. https://doi.org/10.1039/c4ja00458b

Travin, V.V., 2015. The structural position and age of eclogite rocks in the area of Gridino village in the Belomorian mobile belt. Geotectonics 49, 425–438. https://doi.org/10.1134/S0016852115050064

Travin, V.V., Kozlova, N.E., 2009. Eclogitization of basites in early proterozoic shear zones in the area of the village of Gridino, western Belomorie. Petrology 17, 684–706. https://doi.org/10.1134/S0869591109070042

Valley, J.W., Bindeman, I.N., Peck, W.H., 2003. Empirical calibration of oxygen isotope fractionation in zircon. Geochim. Cosmochim. Acta 67, 3257–3266. https://doi.org/10.1016/S0016-7037(00)00090-5

Valley, J.W., Kitchen, N., Kohn, M.J., Niendorf, C.R., Spicuzza, M.J., 1995. UWG-2, a garnet standard for oxygen isotope ratios: Strategies for high precision and accuracy with laser heating. Geochim. Cosmochim. Acta 59, 5223–5231. https://doi.org/10.1016/0016-7037(95)00386-X

Valley, J.W., Lackey, J.S., Cavosie, A.J., Clechenko, C.C., Spicuzza, M.J., Basei, M.A.S., Bindeman, I.N., Ferreira, V.P., Sial, A.N., King, E.M., Peck, W.H., Sinha, A.K., Wei, C.S., 2005. 4.4 billion years of crustal maturation: Oxygen isotope ratios of magmatic zircon. Contrib. to Mineral. Petrol. 150, 561–580. https://doi.org/10.1007/s00410-005-0025-8

van Hunen, J., Moyen, J.-F., 2012. Archean Subduction: Fact or Fiction? Annu. Rev. Earth Planet. Sci. 40, 195–219. https://doi.org/10.1146/annurev-earth-042711-105255

Vho, A., Rubatto, D., Putlitz, B., Bouvier, A.-S., 2020. New reference materials and assessment of matrix effects for SIMS measurements of oxygen isotopes in garnet. Geostand. Geoanalytical Res. 44, 459-471. doi:10.1111/ggr.12324.

Volodichev, O.I., Slabunov, A.I., Bibikova, E. V., Konilov, A.N., Kuzenko, T.I., 2004. Archean eclogites in the Belomorian mobile belt, Baltic Shield. Petrology 12, 540–560.

Watson, E.B., Wark, D.A., Thomas, J.B., 2006. Crystallization thermometers for zircon and rutile.

Contrib. to Mineral. Petrol. 151, 413–433. https://doi.org/10.1007/s00410-006-0068-5

Weller, O.M., St-Onge, M.R., 2017. Record of modern-style plate tectonics in the Palaeoproterozoic Trans-Hudson orogen. Nat. Geosci. 10, 305–311. https://doi.org/10.1038/ngeo2904

Whitney, D.L., Evans, B.W., 2010. Abbreviations for names of rock-forming minerals. Am. Mineral. 95, 185–187. https://doi.org/10.2138/am.2010.3371

Wiedenbeck, M., Allé, P., Corfu, F., Griffin, W.L., Meier, M., Oberli, F., von Quadt, A., Roddick, J.C., Spiegel, W., 1995. Three natural zircon standards for U-Th-Pb, Lu-Hf, trace element and REE analyses. Geostand. Newsl. 19, 1-23. https://doi.org/10.1111/j.1751-908X.1995.tb00147.x

Wiedenbeck, M., Hanchar, J.M., Peck, W.H., Sylvester, P., Valley, J., Whitehouse, M., Kronz, A., Morishita, Y., Nasdala, L., 2004. Further Characterisation of the 91500 Zircon Crystal. Geostand. Geoanalytical Res. 28, 9–39. https://doi.org/10.1111/j.1751-908X.2004.tb01041.x

Williams, I.S., 1998. U-Th-Pb geochronology by ion microprobe. In: McKibben, M.,A., Shanks III, W.C., Ridley, W.I. (Eds), Application of microanalytical techniques to understanding mineralizing processes. Reviews in Economic Geology, Society of Economic Geologists 7, 1-35

Yu, H., Zhang, L., Lanari, P., Rubatto, D., Li, X., 2019a. Garnet Lu–Hf geochronology and P-T path of the Gridino-type eclogite in the Belomorian Province, Russia. Lithos 326–327, 313–326. https://doi.org/10.1016/j.lithos.2018.12.032

Yu, H., Zhang, L., Zhang, L., Wei, C., Li, X., Guo, J., Bader, T., Qi, Y., 2019b. The metamorphic evolution of Salma-type eclogite in Russia: Constraints from zircon/titanite dating and phase equilibria modeling. Precambrian Res. 326, 363–384. https://doi.org/10.1016/j.precamres.2018.01.019

Yu, H.L., Zhang, L.F., Wei, C.J., Li, X.L., Guo, J.H., 2017. Age and P–T conditions of the Gridino-type eclogite in the Belomorian Province, Russia. J. Metamorph. Geol. 35, 855–869. https://doi.org/10.1111/jmg.12258